AFOSR-TR- 80-0002

8

AD A054288

LEVEL III

AD A079658

DDC FILE COPY

DDC
RECEIVED
JAN 18 1980
A

Approved for public release;
distribution unlimited.

80 1 16 055

Cont'

the inversion indicate that a 3 layer, 40 km thick crust is an adequate model consistent with the data for the South-China subplate. Crustal shear velocities are found to be higher and upper mantle shear velocities lower than previously reported values for this region.

Unclassified

UNCLASSIFIED

SECURITY CLASSIFICATION OF THIS PAGE (When Data Entered)

REPORT DOCUMENTATION PAGE	READ INSTRUCTIONS BEFORE COMPLETING FORM
1. REPORT NUMBER: AFOSR-TR-80-0002	2. GOVT ACCESSION NO.
3. RECIPIENT'S CATALOG NUMBER	9 Semi-annual
4. TITLE (and Subtitle): CRUSTAL AND UPPER MANTLE VELOCITY & Q STRUCTURES OF MAINLAND CHINA	5. TYPE OF REPORT & PERIOD COVERED: Interim Technical rept.
	6. PERFORMING ORG. REPORT NUMBER
7. AUTHOR(s): Ta-liang Teng	8. CONTRACT OR GRANT NUMBER(s): F49620-76-C-0010, AFOSR ARPA Order-3291
9. PERFORMING ORGANIZATION NAME AND ADDRESS: Department of Geological Sciences, University of Southern California, Los Angeles, CA 9007	10. PROGRAM ELEMENT, PROJECT, TASK AREA & WORK UNIT NUMBERS: 62701E 9F10 A.O.3291-21
11. CONTROLLING OFFICE NAME AND ADDRESS: ARPA/NMR, 1400 Wilson Blvd., Arlingtcn, VA 22209	12. REPORT DATE: Oct 1978
	13. NUMBER OF PAGES: 83
14. MONITORING AGENCY NAME & ADDRESS(if different from Controlling Office): AFOSR/NP, Bolling AFB, Bldg.410, Wash DC 20332	15. SECURITY CLASS. (of this report): unclassified
	15a. DECLASSIFICATION/DOWNGRADING SCHEDULE

16. DISTRIBUTION STATEMENT (of this Report)

Approved for public release; distribution unlimited.

16 3291

17 21

17. DISTRIBUTION STATEMENT (of the abstract entered in Block 20, if different from Report)

18. SUPPLEMENTARY NOTES

19. KEY WORDS (Continue on reverse side if necessary and identify by block number)

408856 Gm

20. ABSTRACT (Continue on reverse side if necessary and identify by block number)

New data from the Seismological Research Observatory (SRO) is used in conjunction with a nonlinear least squares technique to invert surface wave group velocity data for the shear velocity structure of the South-Cnina subplate. A multi-filter analysis was used to produce group velocities for the fundamental mode Love and Rayleigh wave. A number of earthquakes over a single path are used in order to deduce a measure of the observational uncertainty of the present method. Group velocity standard deviations range from .03 to .1 km/sec for Love waves over the period range of 10 to 65 seconds. Results of

cont'd

DD FORM 1 JAN 73 1473 EDITION OF 1 NOV 65 IS OBSOLETE

UNCLASSIFIED

SEMI-ANNUAL TECHNICAL REPORT

submitted to the

AIR FORCE OFFICE OF SCIENTIFIC RESEARCH

by the

GEOPHYSICAL LABORATORY

UNIVERSITY OF SOUTHERN CALIFORNIA

Contractor:	University of Southern California
Effective Date of Contract:	July 2, 1976
Expiration Date of Contract:	October 31, 1978
Amount of Contract:	$84,403.00
Contract Number:	F49620-76-C-0010
Principal Investigator:	Ta-liang Teng (213) 741-6124
Program Manager:	Bill Best Bolling Air Force Base
Title:	CRUSTAL AND UPPER MANTLE VELOCITY & Q STRUCTURES OF MAINLAND CHINA
Sponsored by:	Advanced Research Projects Agency (DOD) ARPA Order No. 3291 Monitored by AFOSR

CONTENTS

LIST OF ILLUSTRATIONS

APPENDIX FIGURES

LIST OF TABLES

APPENDIX TABLE

ABSTRACT

New data from the Seismological Research Observatory (SRO) is used in conjunction with a non-linear least squares technique to invert surface wave group velocity data for the shear velocity structure of the South-China subplate. A multi-filter analysis was used to produce group velocities for the fundamental mode Love and Rayleigh wave. A number of earthquakes over a single path are used in order to deduce a measure of the observational uncertainty of the present method. Group velocity standard deviations range from .03 km/sec to .15 km/sec for Rayleigh waves and .03 to .1 km/sec for Love waves over the period range of 10 to 65 seconds.

Results of the inversion indicate that a 3 layer, 40 km thick crust is an adequate model consistent with the data for the South-China subplate. Crustal shear velocities are found to be higher and upper mantle shear velocities lower than previously reported values for this region.

INTRODUCTION

The China mainland consists of a number of tectonic subplates, each of geologically and geophysically distinct structures. Based on an investigation of the surface geology, Sun and Teng (1977) divide China into 4 basic tectonic units (Figure 1): (1) the Ching-Tibet subplate, (2) the North-China subplate, (3) the Northwest-China subplate, and (4) the South-China subplate. The present study focuses its attention on the South-China subplate. Specifically it makes use of a group of closely spaced earthquakes which give a number of pure-path surface wave trains recorded at a single SRO station. The resulting dispersion curves give a measure of the observational uncertainty of the surface wave data.

Using a non-linear least squares procedure based on the stochastic model (Franklin, 1970, Jordan and Franklin, 1970, and Derr et al., 1970), intermediate- and long-period group velocity data were inverted to obtain a detailed shear velocity model for the crustal and upper mantle structure of the South-China subplate (SOCHSP). Recently a number of large earthquakes and aftershocks have occurred at the boundary between the Ching-Tibet subplate and the South-China subplate. These events have been recorded at an SRO station at Taipei, Taiwan with

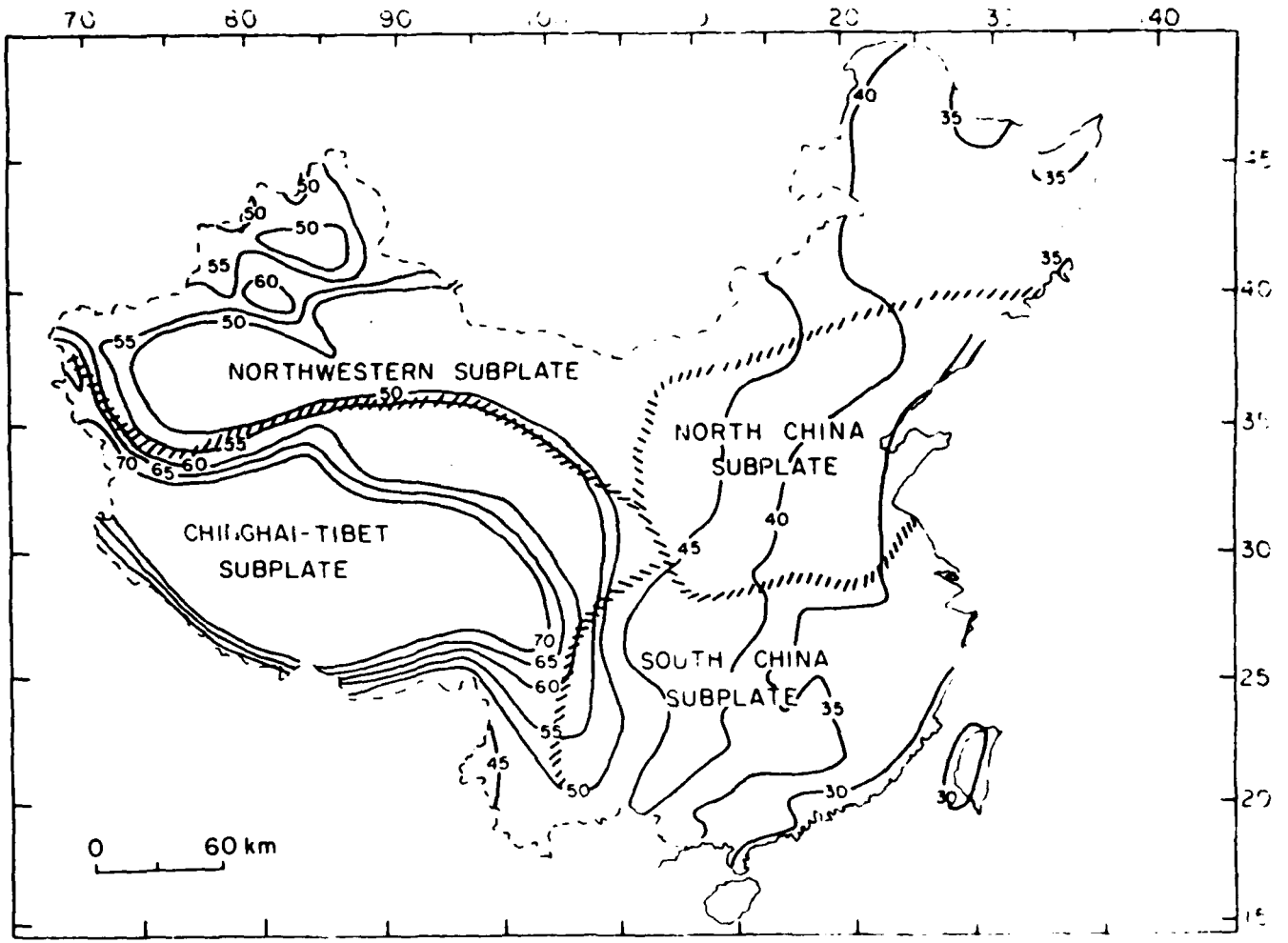

FIGURE 1. TECTONIC SUBPLATES OF CHINA

the station code TATO. SOCHSP is ideally suited for a surface wave study for three reasons: (1) the South-China subplate can be considered nearly laterally homogeneous (Tung, 1974; Sun and Teng, 1977); epicentral distances are adequate to allow an intermediate to long period dispersive wave train to develop; (3) seismic events occur and are recorded within the subplate, thus eliminating the effects of crossing plate boundaries.

Lacking good geophysical data, most of the previous seismological studies were either limited to a simple estimate on the crustal thicknesses and shallow crustal structures or lacked a discussion of model resolution and standard deviation. Knowledge about the crustal and mantle shear velocity structure of SOCHSP is poor. Tseng and Sung (1963) determined crustal thickness by applying the tripartite method (Press, 1956) to two events from the New Britain Islands for phase velocity information. The inversion results of their study are seen in Figure 2. The numbers inside each triangle represent the average crustal thickness within three stations. Using short period (4-12 seconds) Rayleigh and Love wave group velocity dispersion, Sung et al. (1965) determined the thickness of the sedimentary layers for several regions in China. Tung (1974) made use of long period group velocity data and tried to obtain a shear velocity structure for SOCHSP. But the method he used was

FIGURE 2

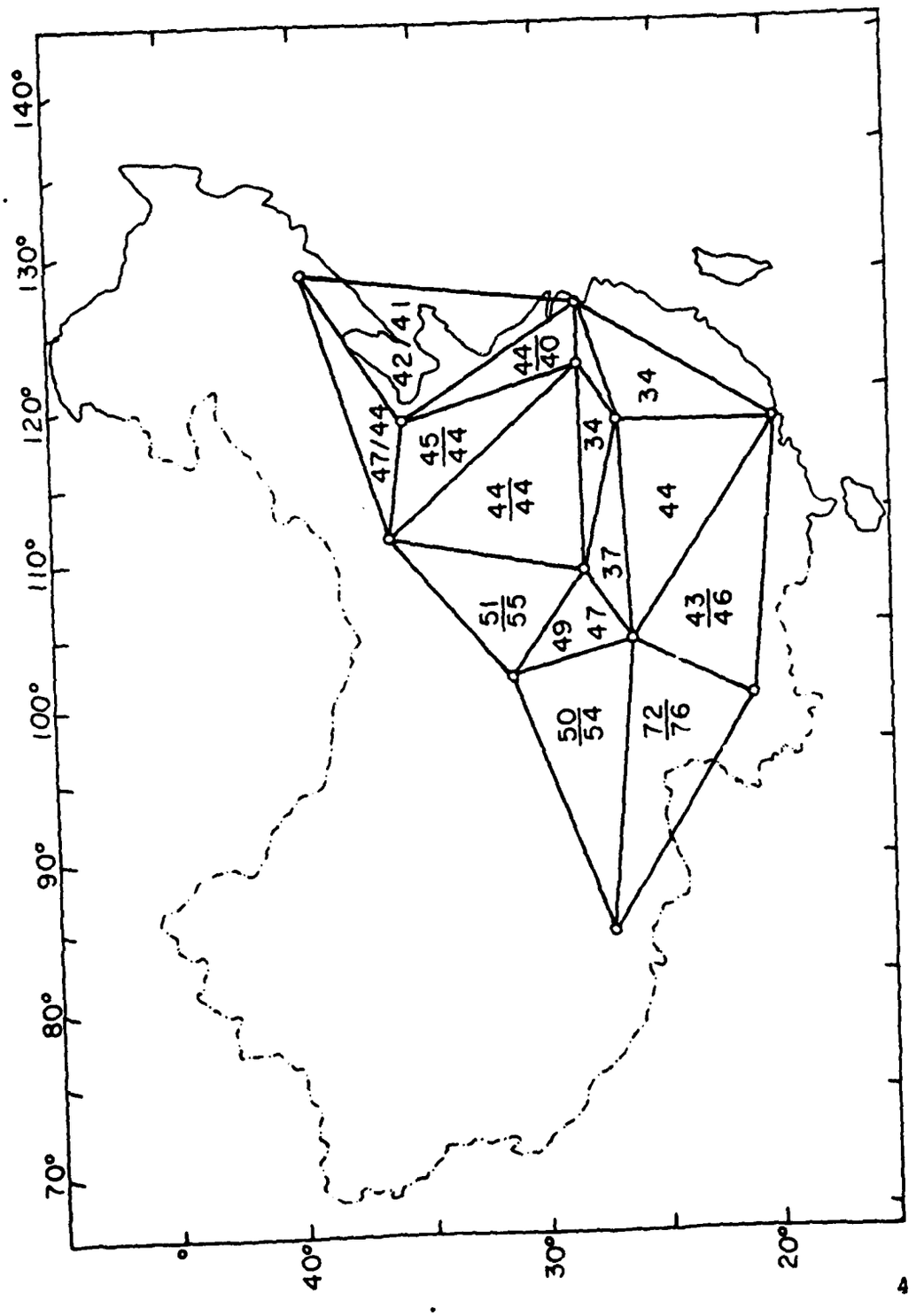
140°
130°
120°
110°
100°
90°
80°
70°
40°
30°
20°
42/41
44/40
34
47/44
45/44
34
44/44
44
37
51/55
49
47
43/46
50/54
72/76

essentially a trial-and-error surface wave inversion technique and thus he was unable to give a discussion about resolution or standard deviation of his resulting models.

Previous work has illustrated that Rayleigh waves produce more information about earth models than Love waves (Wiggin, 1972; Derr and Landisman, 1972). Wiggins (1972) has shown that by simultaneously inverting Love and Rayleigh wave data, it is possible to obtain both shear wave and density structures. Though group velocity and phase velocity contribute almost the same information (Bloch, 1969, Bloch et al., 1969, Wiggins, 1972), Bloch (1969) and Fix (1975) come to the conclusion that group velocity is more sensitive to the earth model and therefore should produce better resolution in the inversion. Through a multiple filtering technique, this study first obtains group velocity measurements from the fundamental mode Love and Rayleigh waves, followed by a Gilbert-Backus (1967, 1968) type inversion to obtain a crustal and upper mantle structure of SOCHSP together with an estimate of model standard deviation and resolution.

SOUTH-CHINA SUBPLATE

The South-China subplate (SCS) is bounded on the south and east by the Pacific Ocean, on the west by longitude 103°E, and on the north by latitude 32°N (Figure 3). From previous gravity and seismic studies (Tseng and Sun, 1963; Tseng, 1973; Tung, 1974) the crustal thickness of SCS is believed to increase from 30 km at the eastern boundary to 50 km at the western boundary with an average thickness of 40 km.

The subplate is composed of two parts, the Yangtze fault block in the northwest and the South-China folding block in the southeast. The Yangtze fault block is a section of old continental crust formed during the Jinning Orogeny (1300-950 m.y.), and was subsequently faulted and strongly metamorphosed. Formed during the Caledonian Orogeny (570-400 m.y.), the South-China folding block was a section of transitional (miogeosynclinal) crust that later underwent weak metamorphism and folding. (Tectonic Map Compiling Group, 1974, Guizhou Geologic Team 108, 1975).

While surrounded by a number of seismically active zones, SOCHSP is one of the most stable regions in China. Though a number of large events occur on or beyond its western boundary, which marks the India-Eurasia collision,

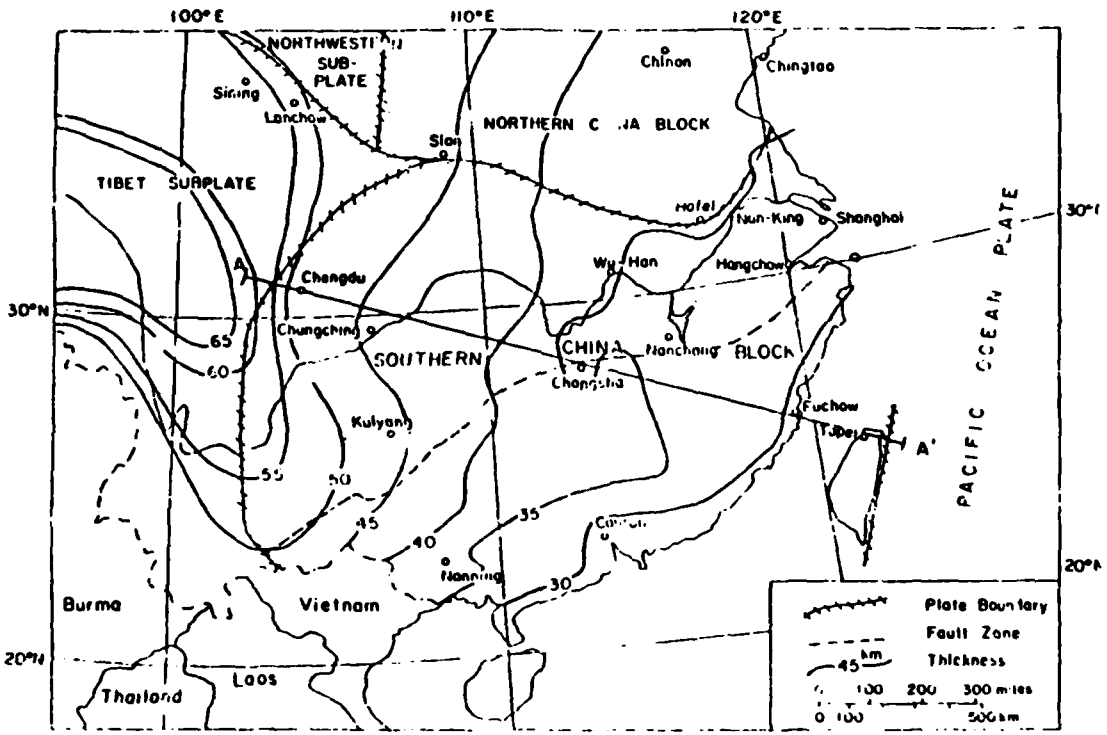

FIGURE 3. THE SOUTH-CHINA SUBPLATE

there are only a few interplate earthquakes (Figure 4). According to Li et al. (1974), this can be explained by the fact that this region has undergone weaker metamorphism than other regions and therefore, the rocks are softer and do not lend themselves to high stress accumulation.

DATA

The data used in this study are surface waves from four earthquakes (Table 1) focused in the Szechwan Province of mainland China. The events were recorded at SRO station TATO. A number of events over one path were desired in order to establish data repeatability and to obtain observational uncertainties. Because of instrument problems and poor dispersion results (due to the arrival of wave energy at certain periods that have taken non-least-time paths), certain components of individual earthquakes were not used in obtaining group velocity information. The epicentral region and path are shown in Figure 3 (4-4').

SRO data in digital form on tape is convenient for computer processing techniques and the storage of a large amount of information on a single data tape. The SRO station operates at high sensitivity thus expanding the detection threshold for seismic events making small magnitude events ($M \sim 5$) useful for surface wave analyses.

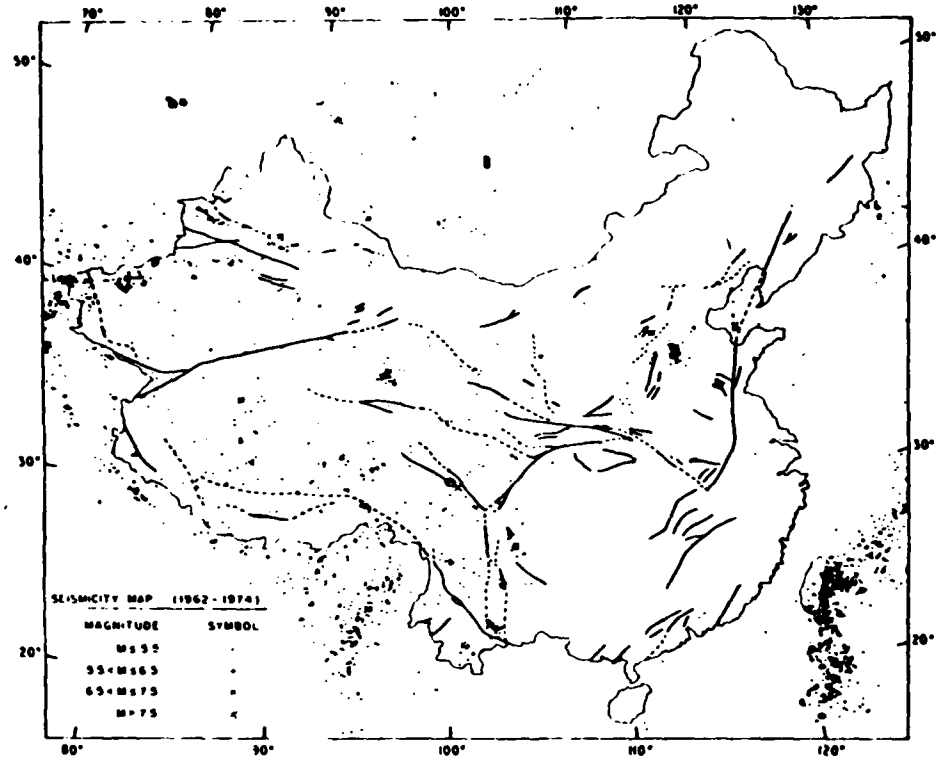

Map showing distribution of epicenters of recent earthquakes in China (1962–1974) using Albers equal-area projection.

FIGURE 4

TABLE 1

LIST OF SEISMIC EVENTS

Date	Location	Focal Depth (km)	Magnitude	Epicentral Distance (km)
August 19, 1976	32.893N 104.189E	33	5.4	1902.0
August 22, 1976	32.992N 104.181E	33	4.7	1884.0
September 1, 1976	32.460N 104.152E	18	5.1	1886.0
September 3, 1976	28.040N 100.345E	33	5.2	1854.0

With this new system, the amount of data available for long-period surface waves studies is greatly increased.

SRO datatapes contain data from three long-period channels, sampled at the rate of once per second and one vertical component sampled at the rate of twenty times per second. Long-period data is recorded continuously on tape; short-period data is recorded only when an event has been detected, and is sampled at the rate of twenty times a second. The vertical, north-south, and east-west long period channels are multiplexed into each record. Each SRO data record consists of 1000 words (2000 bytes). The first ten words are header information. The next 990 words are data; therefore, there are 5 minutes, 30 seconds of data per long period record (Peterson et al., 1976).

The amplitude and phase response for the long-period instrument is given in Table 2. An analytic form of the transfer function used in our computer program is found by numerically fitting the amplitude and phase response into a polynomial. The transfer function has the form:

$$\frac{\sum_{i}^{n} a_i z^i}{\sum_{i}^{n} b_i z^i}$$

where: $a_0 = 1.7443 \times 10^{-4}$ $a_1 = 3.1635 \times 10^{-3}$

$a_2 = .21163$ $a_3 = .14127$

TABLE 2

Frequency	Relative Amplitude	Phase Angle (Radians)
.0667	.460	-1.33
.05556	.672	-1.00
.04546	.912	-0.63
.04	1.00	-0.42
.0333	1.01	-0.13
.02778	.9	0.10
.02326	.724	0.30
.02	.550	0.47
.01667	.400	0.63
.0125	.200	0.92
.01	.108	1.10
.00667	.031	1.34
.005	.0104	1.51
.0025	.00084	1.84
.00167	.000184	2.00

$b_0 = 3.531 \times 10^{-}$ $b_1 = 3.3316 \times 10^{-2}$

$b_2 = .12378$ $b_3 = 1.0$

A plot of this transfer function is given in Figure 5.

Each seismic event must be decoded and plotted from the data tapes. Pure Love waves are obtained by rotating the data coordinates. An example of a plotted seismic event before and after coordinate rotation is given in Figure 6 and 7.

A multiple filtering analysis (Dziewonski and Hales, 1970; Hermann, 1973; Tung, 1974; Seekins and Teng, 1976) has been applied to the surface wave train to obtain group velocity dispersion curves. A typical contoured result of this type of analysis is shown in Figure 8. Because of the epicentral distances involved, only periods of up to 65 seconds were used for Rayleigh waves and 50 seconds for Love waves. The dispersion curves for the fundamental mode Love and Rayleigh waves are plotted in Figures 9 and 10. In these figures, the solid line represents the average group velocities obtained from the multiple filtering analysis. The statistical properties of the observations are listed in Table 3 and 4.

THEORY

Generalized least squares methods for determining the Earth's structure from seismic data have been formulated by

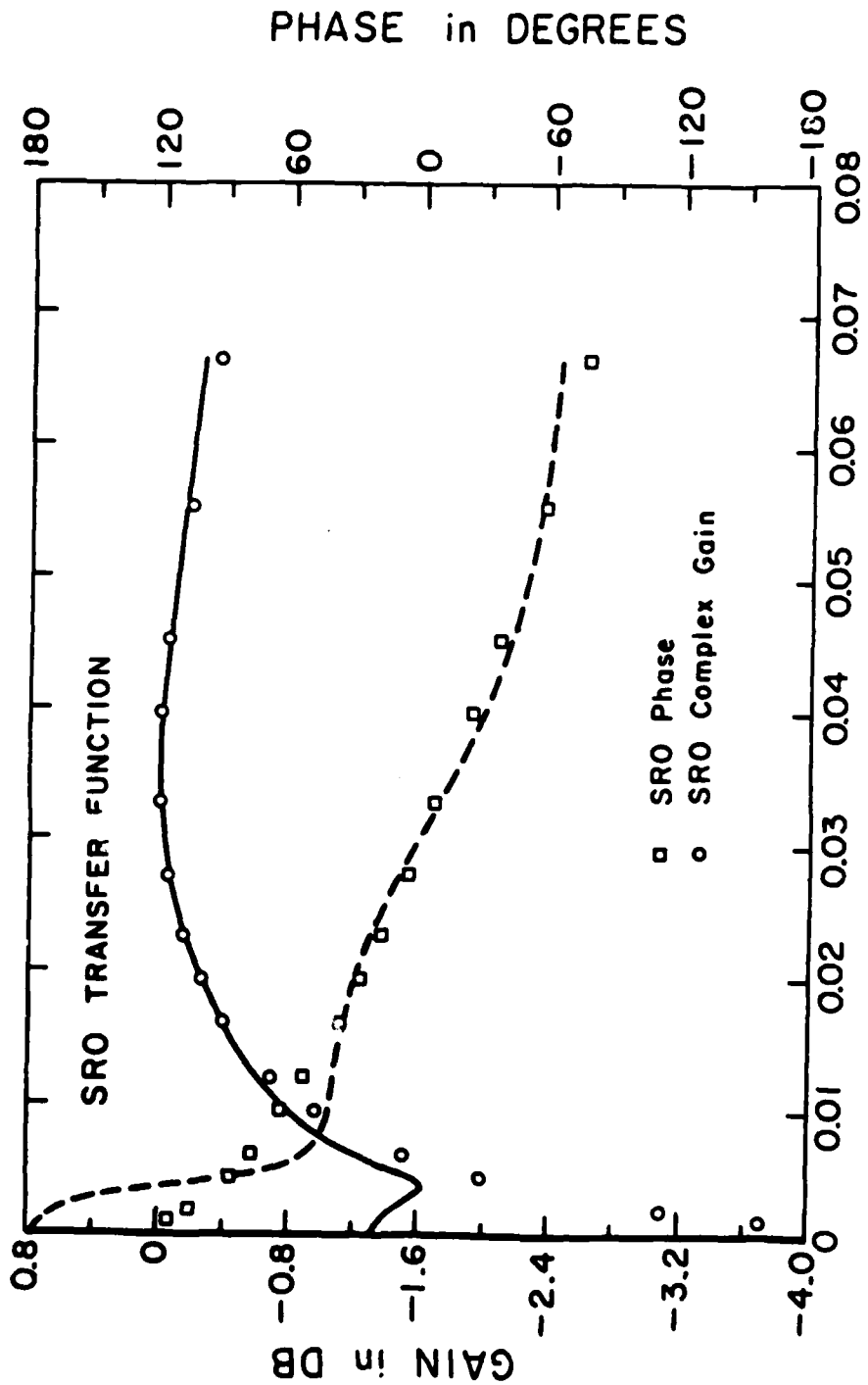
PHASE in DEGREES
180
120
60
0
-60
-120
-180
SRO TRANSFER FUNCTION
SRO Phase
SRO Complex Gain
FREQUENCY
0.01
0.02
0.03
0.04
0.05
0.06
0.07
0.08
GAIN in DB
0.8
0
-0.8
-1.6
-2.4
-3.2
-4.0

FIGURE 5

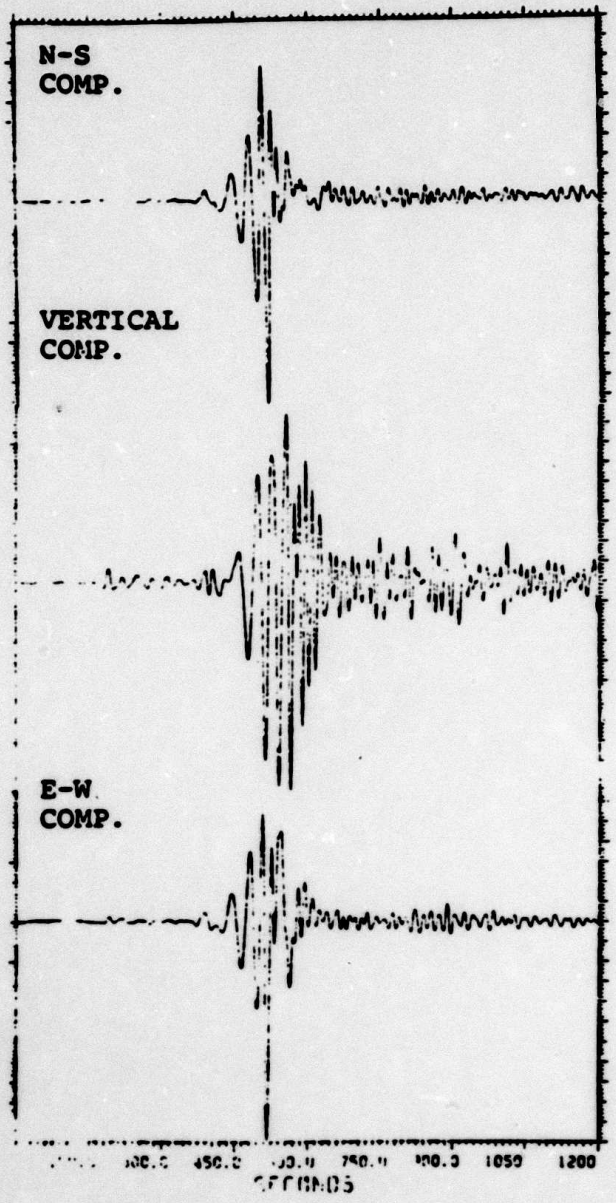

FIGURE 6

UNROTATED SEISMOGRAM 8/18/76

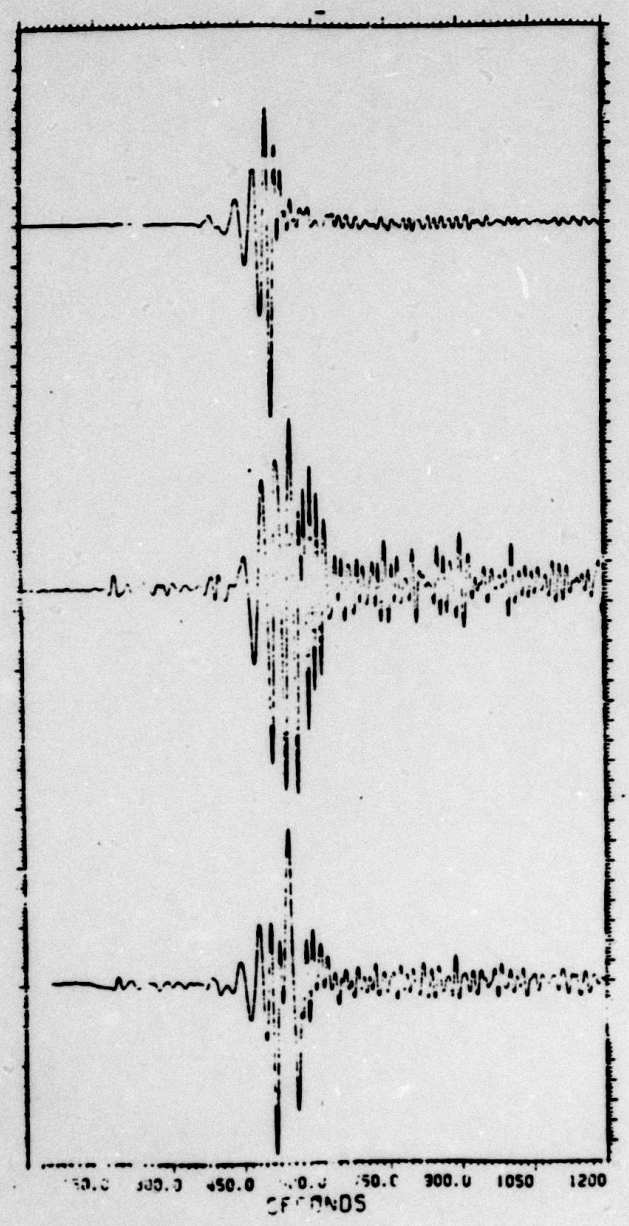

FIGURE 7

ROTATED SEISMOGRAM 8/18/76

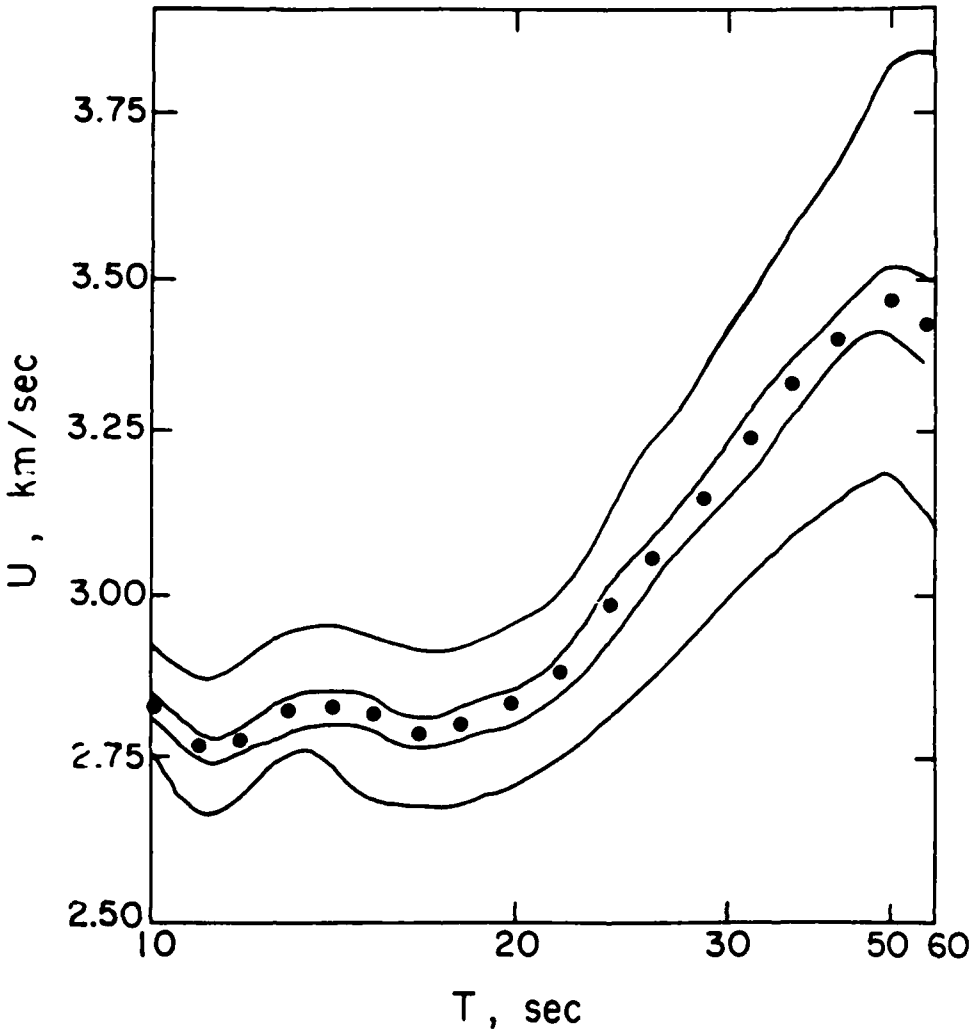

FIGURE 8
MULTI-FILTER ANALYSIS OF VERTICAL COMPONENT
9/1/76

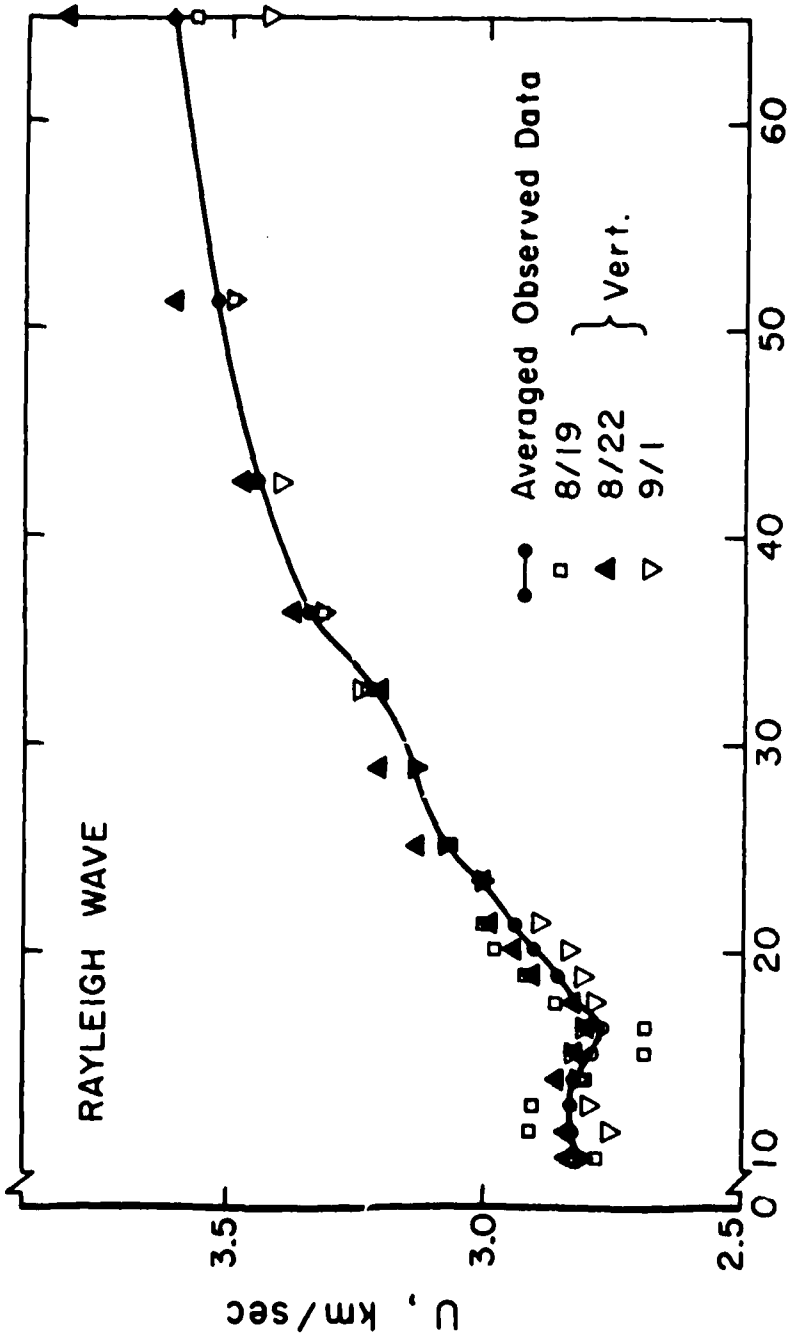
RAYLEIGH WAVE
Averaged Observed Data
8/19
8/22
9/1
Vert.
U , km/sec
T, sec
3.5
3.0
2.5
0
10
20
30
40
50
60

FIGURE 9

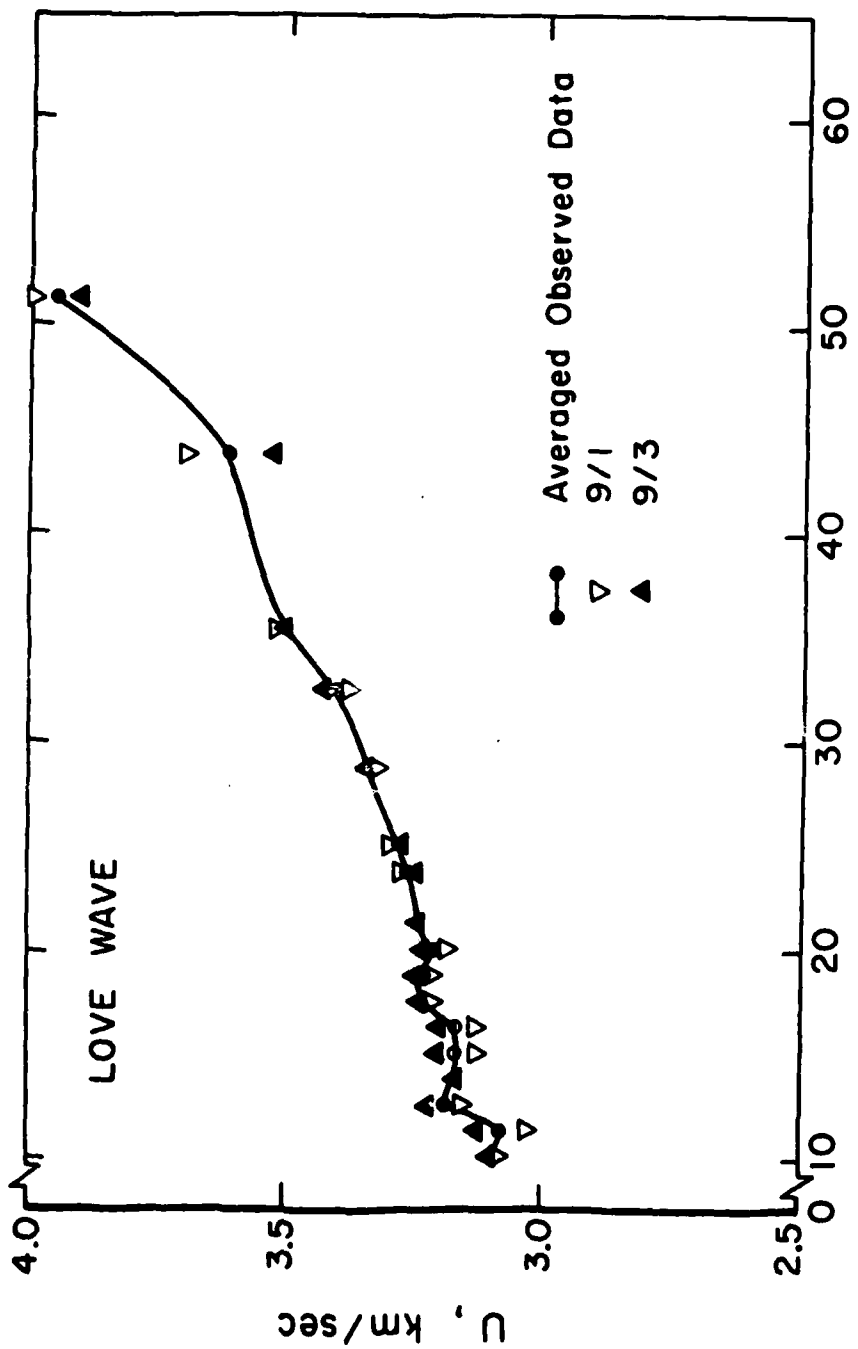
LOVE WAVE
Averaged Observed Data
9/1
9/3
U , km/sec
T , sec
4.0
3.5
3.0
2.5
0
10
20
30
40
50
60

FIGURE 10

TABLE 3

RAYLEIGH WAVE

PERIOD	AVERAGED OBSERVED GROUP VELOCITY (KM/SEC)	ESTIMATED STANDARD DEVIATION
64.00	3.61	.15
51.20	3.54	.07
42.667	3.44	.04
36.571	3.35	.03
32.00	3.23	.03
28.444	3.14	.03
25.60	3.07	.03
21.333	2.95	.06
19.692	2.91	.06
18.286	2.86	.05
17.067	2.83	.05
16.00	2.77	.07
15.059	2.78	.07
13.474	2.83	.03
12.19	2.83	.06
11.13	2.83	.06
10.24	2.81	.03

TABLE 4

LOVE WAVE

PERIOD	AVERAGED OBSERVED GROUP VELOCITY (KM/SEC)	STANDARD DEVIATION
51.2	3.95	0.1
42.667	3.61	0.1
36.571	3.52	.03
32.00	3.41	.03
28.444	3.35	.03
25.60	3.29	.03
23.273	3.26	.03
21.333	3.24	.03
19.692	3.22	.03
18.286	3.24	.03
17.067	3.23	.03
16.00	3.17	.04
15.059	3.17	.05
13.474	3.17	.03
12.19	3.19	.04
11.13	3.08	.06
10.24	3.09	.03

numerous authors (Jackson, 1972; Wiggins, 1972; and Crosson, 1976). The basic logic in the inversion theory is as follows:

The observations, Y_i, are related to certain model parameters, X_j, in some known way, $Y_i = A(X_1, X_2, \ldots X_p)$. A quasi-linear relationship is established by taking a Taylor series expansion about some initial value X_0'.

$$Y_i = A_i(X_0') + \frac{\partial A_i}{\partial X_j} \Big|_{X_0'} \Delta X + \text{higher order terms}$$

$$Y_i \equiv A_i(X_0') + \Delta Y_i$$

Ignoring the higher order terms, we obtain the functional relationship:

$$\Delta Y_i = \frac{\partial A_i}{\partial X_j} \Big|_{X_0'} \Delta X_j \qquad (1)$$

where ΔY_i = observed data minus calculated observations. Equation 1 in matrix form becomes:

$$A\Delta X = \Delta Y$$

Where A is a matrix whose elements are the partial derivatives in Equation 1, ΔX is a p x 1 vector whose elements are correction to the initial model vector X_0', and ΔY is the difference between the observed and theoretical data.

In our case the observations are group velocities of

Love and Rayleigh waves, and the model parameters are shear velocities and densities for a horizontally layered earth. The partial derivatives in equation 1 are generated numerically by the method described by Rodi et al. (1975).

The classic least squares solution to equation 2 is by minimizing the euclidean length of $A\Delta X-\Delta Y$ or

$$|| A\Delta X-\Delta Y || = (A\Delta X-\Delta Y)^T(A\Delta X-\Delta Y) = \varepsilon$$

Given equation 2, the solution is (Hanson and Lawson, 1975):

$$A\Delta X = \Delta Y$$
$$A^TA\Delta X = A^T\Delta Y$$
$$\Delta\hat{X} = (A^TA)^{-1}A^T\Delta Y$$

where $\Delta\hat{X}$ is the estimated correction vector.

A suitable inverse to this problem can be obtained by using the singular value decomposition (SVD) of the matrix A.

$$A = U\Lambda V^T$$

where the columns of U are the eigenvectors associated with the colums of A, the rows of V are the eigenvectors associated with the rows of A, and Λ is a diagonal matrix of non-zero eigenvalues of the matrix A.

$$\Lambda = A^T A = \begin{vmatrix} \lambda_1 & \cdot & \cdot & \cdot & \cdot \\ 0 & \lambda_2 & \cdot & \cdot & \\ \cdot & \cdot & \cdot & \cdot & \cdot \\ 0 & \cdot & \cdot & \cdot & \lambda \end{vmatrix}$$

If we let

$$H = (A^T A)^{-1} A^T \tag{3a}$$

then

$$HA\Delta X = H\Delta Y \tag{3b}$$

and

$$\Delta\hat{X} = HA\ X \tag{3c}$$

and

$$\Delta\hat{X} = H\Delta Y$$

Using the SVD we obtain (Jackson, 1972):

$$\Delta\hat{X} = (\Lambda V^{-1} U^T)\Delta Y \tag{3d}$$

$$H = \Lambda V^{-1} U^T$$

Here, H is known as the pseudo-inverse of equation 2.

The matrix product HA=R is known as the resolution matrix, and is a measure of the uniqueness of the solution (Jackson, 1972). The rows of R are called the resolving kernals. From equation 3c, it can be seen that an element of $\Delta\hat{X}$, $\Delta\hat{X}_i$, may be interpreted as convolving the i^{th} row of R with the vector ΔX. Therefore, ΔX_i can be considered the weighted sum of nearby values (Jackson, 1972).

Because A^TA is nearly singular, a number of problems arise: (1) The solution vector becomes large which can cause the problem to leave the region of linearity; (2) the solution oscillates with each iteration. By looking at the pseudo-inverse H we can see the cause of this instability.

$$H = V\Lambda^{-1}U^T$$

where the matrix Λ^{-1} equals

$$\Lambda^{-1} = \begin{vmatrix} \frac{1}{\lambda_1} & 0 & \cdot & \cdot & \cdot & \cdot \\ 0 & \frac{1}{\lambda_2} & 0 & \cdot & \cdot & \cdot \\ \cdot & \cdot & \cdot & \cdot & \cdot & \cdot \\ \cdot & \cdot & \cdot & \cdot & \cdot & \cdot \\ 0 & \cdot & \cdot & \cdot & \cdot & \frac{1}{\lambda_n} \end{vmatrix}$$

and the λ_i's are the eigenvalues of the matrix A^TA. If A^TA is near singular, one or more of the eigenvalues will be approaching zero. From equation 3 it can be seen that a small eigenvalue will cause a large change in one or more values of the correction vector $\hat{\Delta X}$. Similarily, it has been shown that the variance of the model parameters are inversely proportional to λ (Jackson, 1972). Thus small λ's produce large standard deviations.

There are two main approaches to stabilizing the inversion process. One method is to examine the

eigenvalue spectrum of the matrix A. Small eigenvalues are removed when the variance becomes too large. But removing the eigenvalues degrades the resolution. This trade-off between resolution and variance has been discussed by a number of authors (Jackson, 1972; Wiggins, 1972; and Crosson, 1976). Braille and Keller (1975) used this method for the inversion of group velocity data.

Inversion stability can also be achieved by using Marquardt's method (Marquardt, 1963) or the stochastic inverse (Franklin, 1970). These procedures lead to the suppression of small eigenvalues. Franklin's stochastic inverse estimates the parameter in the presence of noise. Equation 2 becomes:

$$A\Delta X + n = \Delta Y \tag{4}$$

where n is a vector of observational noise. Franklin (1970) shows that the solution to equation 4 is given by:

$$\Delta X = WA^T(AWA^T + ED)^{-1}\ \Delta Y \tag{5}$$

where W is the covariance matrix of the parameter and ED is the covariance matrix of the observations.

Marquardt's method considers a minimization of the functional

$$(A\Delta X - \Delta Y)^T(ED^TED)(A\Delta X - \Delta Y) - \Delta X^T(W^TW)\ \Delta X \tag{6}$$

with the solution given by:

$$\Delta X = (A^T E D^{-1} A + W_p^{-1})^{-1} A^T E D^{-1} \Delta Y \qquad (7)$$

Letting $A^T E D^{-1} = A^T$, equation 7 becomes:

$$\Delta X = (A^T A + \sigma^2 I)\ A^T \Delta Y \qquad (8)$$

where σ^2 is the variance of the parameter.

By looking at the SVD of equation 8 we can see how Marquardt's method tapers the eigenvalue spectrum:

$$\Delta X = V \left| (\Lambda^2 + \sigma^2 I)^{-1} \Lambda \right| U^T \Delta Y \qquad (9)$$

An element in brackets from equation 9 equals: (Crosson, 1976)

$$\left| (\Lambda^2 + \sigma^2 I)^{-1} \Lambda \right|_i = \lambda_i / (\lambda^2{}_i + \sigma^2)$$

So as λ_i goes to 0, the parameter ΔX_i goes to zero. A similar analysis for the stochastic inverse shows that it too suppresses small eigenvalues.

The quantity σ^2 can also be thought of as a trade-off parameter between resolution and variance (Der et al., 1970; Wiggins, 1972; Crosson, 1976). In Marquardt's method, the resolution equals (Crosson, 1976):

$$R = HA = (A^T A + \sigma^2 I) A^T A = V \left| (\Lambda + \sigma^2 I)^{-1} \Lambda^2 \right| V^T \qquad (10)$$

For the stochastic inverse

$$R = |(\Lambda^2 + \sigma^2 I)^{-1}\Lambda^2| VV^T \qquad (11)$$

The quantity in brackets of equations 10 and 11 is a diagonal matrix whose elements have the form:

$$\lambda_i^2/(\lambda^2 + \sigma^2)$$

If $\sigma^2 = 0$, then R = I, but as σ^2 goes to 0 the variance of the parameters becomes larger. So we adjust the size of σ^2 until there is an acceptable trade-off between standard deviation and resolution.

Two other elements that must be analyzed in the inversion process are the apriori (SDX_0) and postpriori (*SDX*) *standard deviations of the inversion parameters:*

$$SDX_0 = D^T(\sigma WP^{-1})D$$

$$SDX = \sqrt{D^T(A^T ED^{-1}A + \sigma WP^{-1})^{-1}D}$$

where D = a row vector of a delta matrix = (0,0,...,1,...0). This analysis will give a measure of how much new information is coming from the data. If SDX_0 and SDX are approximately the same, we know that very little information is coming from the data.

The advantages of Marquardt's method and the stochastic inverse is that the SVD of A is not explicitly determined and there is no decision to be made on the rank of the matrix A^TA.

A combination of these two methods are used in our

inversion process. When the number of parameters is greater than the number of data, the stochastic inverse is used. If the number of observations is greater than the number of parameters, Marquardt's method is used. This procedure leads to the minimum number of computations.

DISCUSSION

Initial models for the inversion were based on the results of a previous surface wave study done by Tung and Teng (1974). Their final model was obtained from Love and Rayleigh wave group velocity data. Our starting model (M1, Table 5) was inverted for both shear velocity and density.

During the inversion, large instabilities of the density parameter were found in the crust. This was corrected by changing the starting model and inverting for compressional wave velocity. In the derived model (DM1) a low velocity layer (LVL) can be inferred in the sixth layer, but the validity of this LVL is questionable because of the insufficient data in our study. Examination of the apriori and postpriori standard deviations for the shear velocity parameter (Table 5) shows that there is only a small amount of information in the data applicable to depths below the fifth layer. Thus longer period information is needed to confirm velocities beyond

TABLE 5

STARTING MODEL
M1

LAYER THICKNESS (KM)	D-VELOCITY (KM/SEC)	SHEAR VELOCITY (KM/SEC)	DENSITY
10	5.0	3.0	3.0
10	5.0	3.1	3.05
20	6.0	3.5	3.2
20	8.40	4.6	3.3
25	8.05	4.55	3.34
50	7.80	4.2	3.37
50	8.00	4.3	3.37

FINAL MODEL
DM1

SHEAR VELOCITY (KM/SEC)	SDX_0	SDX
3.245	.277	.046
3.193	.277	.076
3.767	.196	.055
4.498	.196	.106
4.495	.175	.112
4.283	.124	.105
4.435	.124	.120

this depth.

A new initial model (M2) using thinner layers in the crust and mantle was inverted for shear wave velocity, density and compressional wave velocity. The mantle shear velocities for M2 were also modified, as were density and P velocity values in the crust (Table 6).

By examining the relative sizes of the partial derivatives of different parameters, we can determine the importance of each parameter in the inversion. The partial derivatives of group velocity with respect to P wave velocity, shear velocity and density for the fundamental Rayleigh wave mode are plotted in Figure 11a, b, and c. The partial derivatives of group velocity with respect to shear velocity and density are plotted in Figure 12a, b for the fundamental Love wave mode. Figures 11 and 12 show a number of important factors that affect this study:

(1) The partial derivatives for P wave velocity in the upper crust are not insignificant when compared to density and shear velocity and therefore, affect the inversion.

(2) The P wave partial derivatives in the lower crust and mantle are small, and are not significant in the inversion.

(3) The partial derivatives with respect to shear velocity are larger than those for density and P

TABLE 6

STARTING MODEL
M2

LAYER THICKNESS	P-VELOCITY (KM/SEC)	SHEAR VELOCITY (KM/SEC)	DENSITY
5	5.5	3.0	2.8
5	5.5	3.0	2.8
5	5.5	3.1	3.05
5	5.5	3.1	3.05
10	6.0	3.5	3.1
10	6.0	3.5	3.1
10	8.1	4.6	3.3
10	8.1	4.6	3.3
10	8.0	4.4	3.3
15	8.0	4.4	3.3
25	8.0	4.4	3.37
25	8.0	4.4	3.37

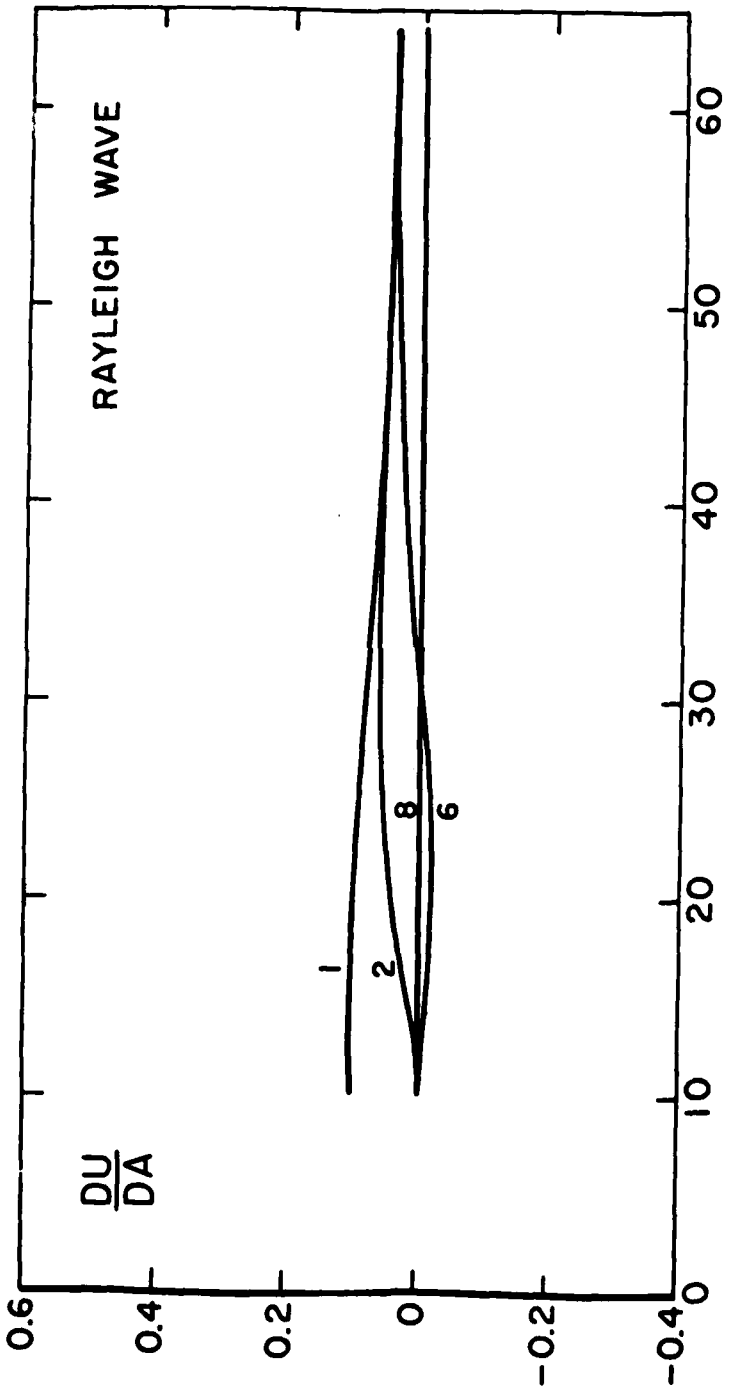

FIGURE 11a

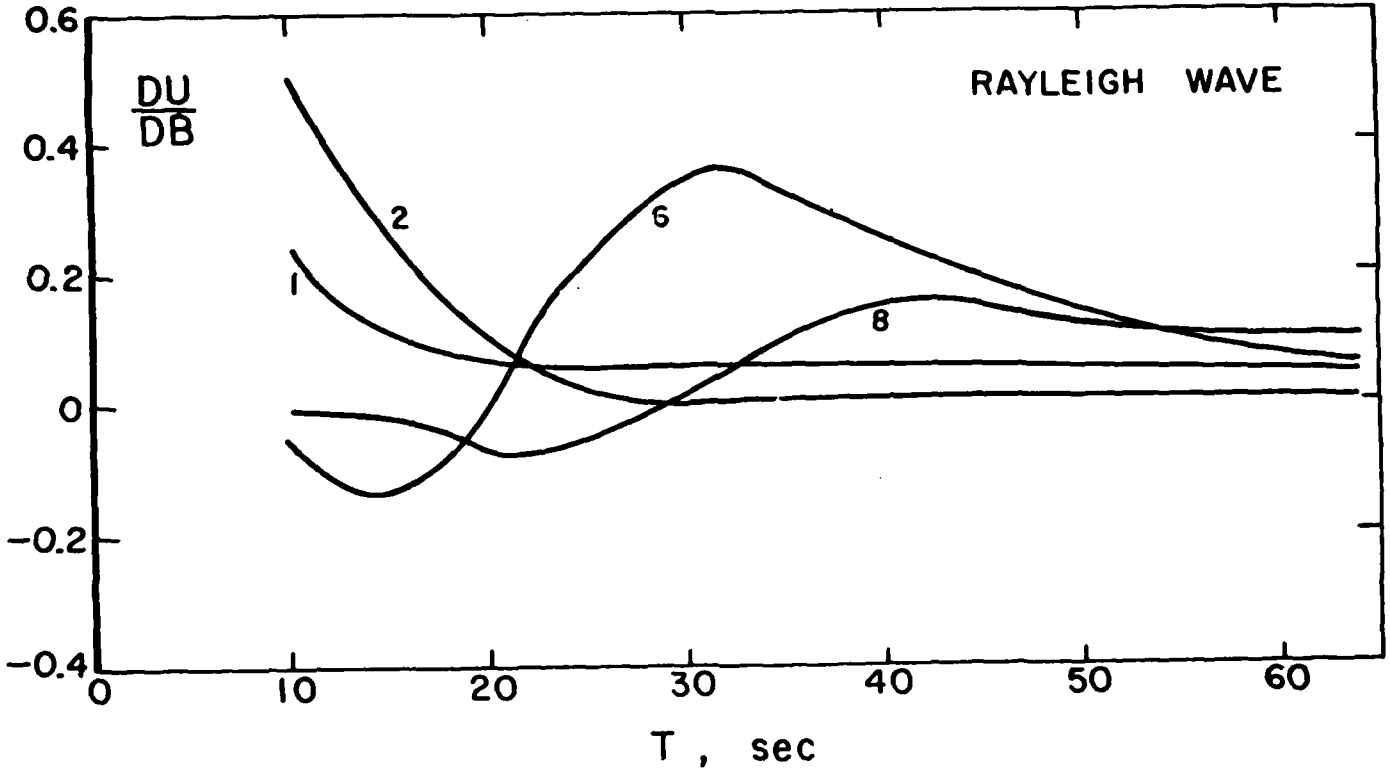

FIGURE 11b

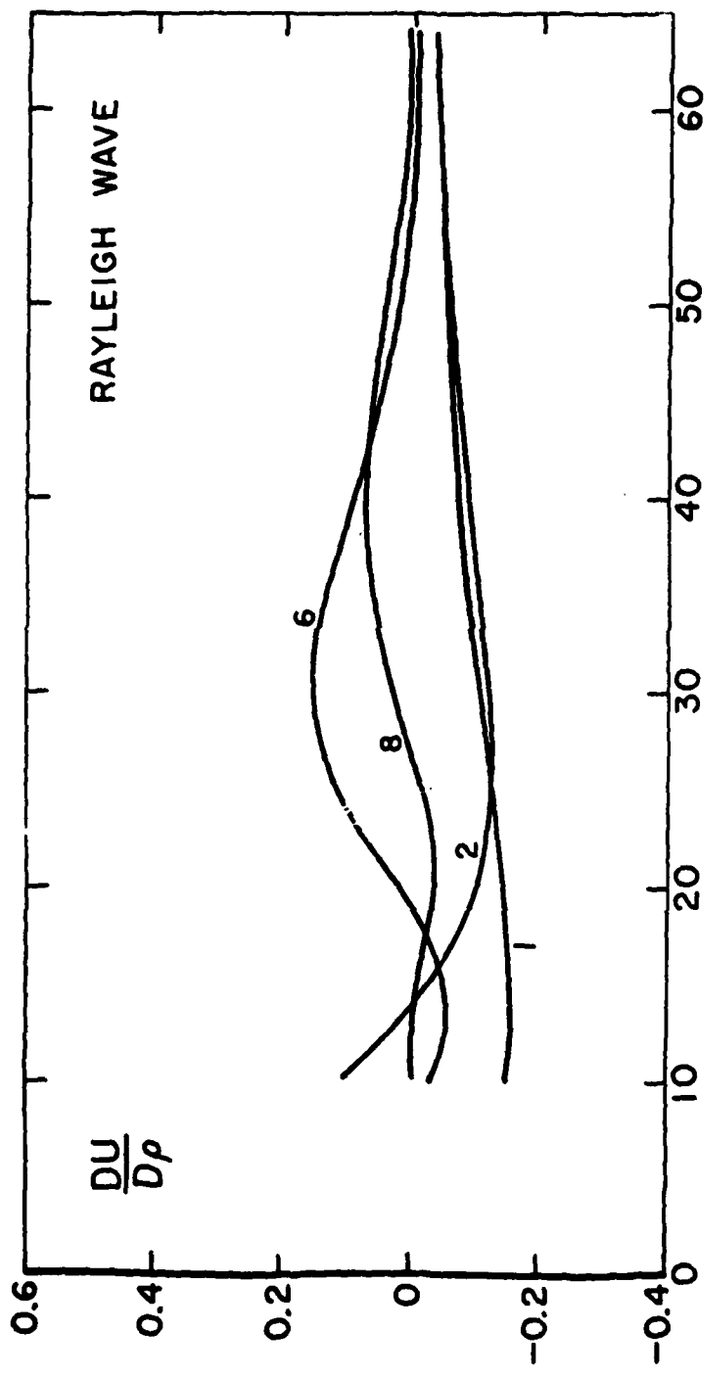
RAYLEIGH WAVE
$\frac{DU}{D\rho}$
0.6
0.4
0.2
0
-0.2
-0.4
0
10
20
30
40
50
60
T , sec
6
8
2
1

FIGURE 11c

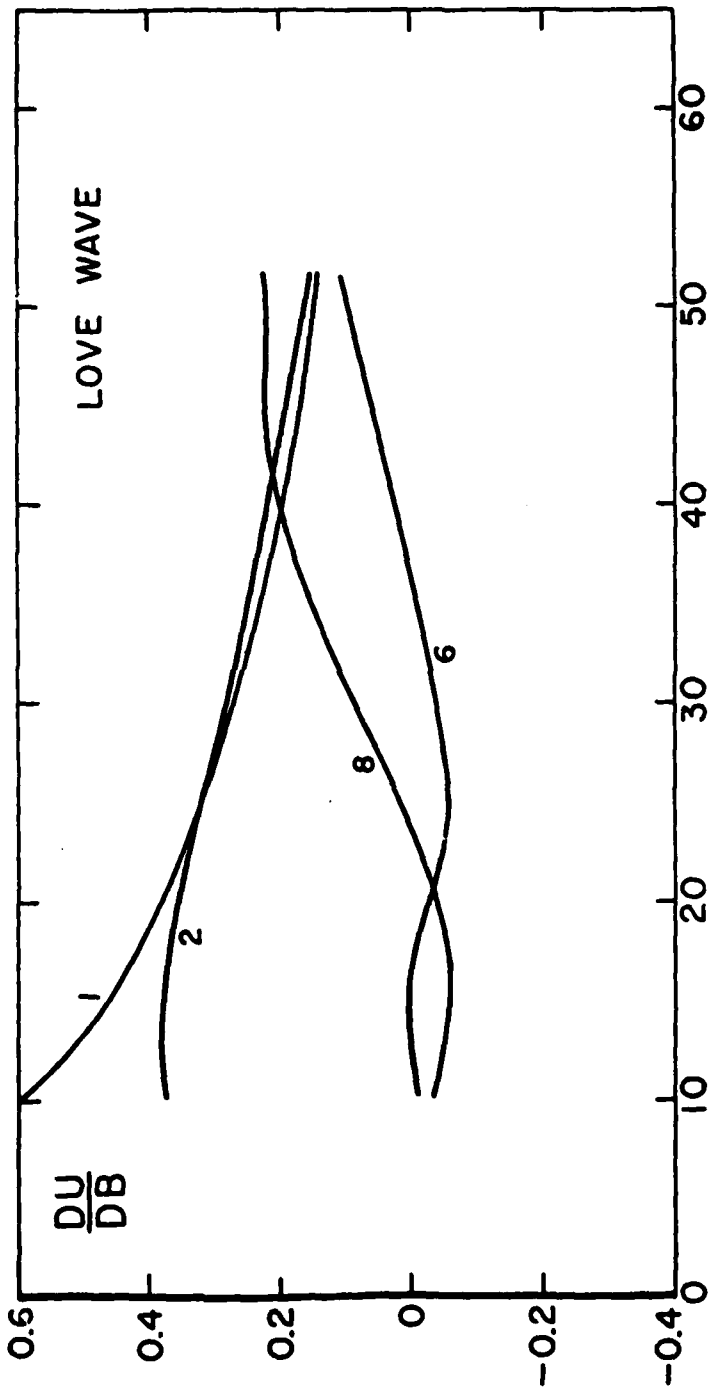

FIGURE 12a

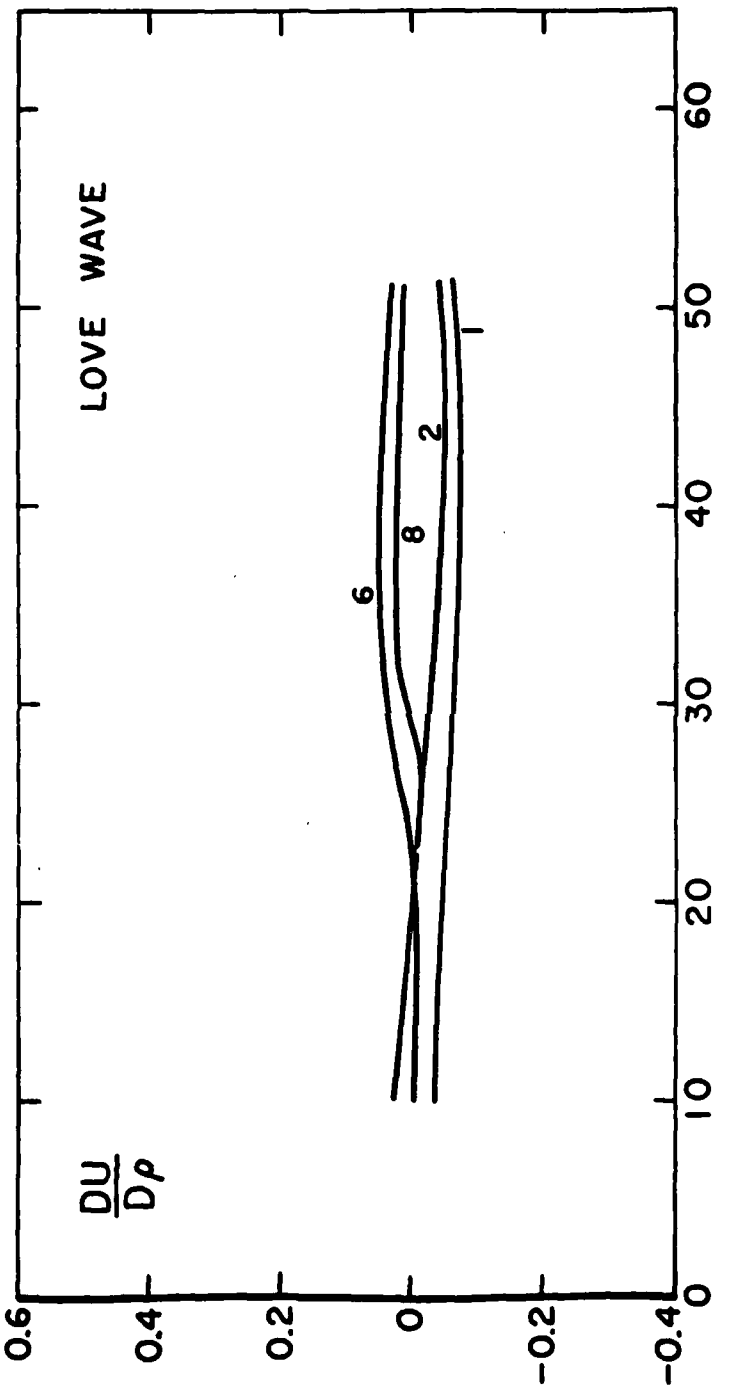

FIGURE 12b

wave velocity. Therefore, the resolution for shear velocities is better than for the two other parameters.

The starting model M2 and the derived model (SCS1) with standard deviation error bars are shown in Figure 13. The fit of theoretical group velocities for SCS1 are shown in Figures 14 and 15. The averaging kernals are listed in Table 7, where only the elements of the kernals corresponding to the shear parameters are included. The other elements for P wave velocity and density are small and do not affect the structure. The width of these kernals indicate that it is possible to resolve layers to a thickness of 5 km in the upper crust, 10 km in the middle crust and 20 km in the lower crust. However, resolution in the mantle is quite poor. All the standard deviations were found to be less than .08 km/sec. Increasing the resolution in the lower crust and mantle (by using a different trade-off parameter σ) leads to instability in the shear velocity model, and unacceptably large standard deviations. These features could be improved if higher mode data were available.

The results of the inversion indicate that only a few layers are justified to describe the crust with the given dispersion information. As an option in the inversion program, averaging kernals can be made to resemble

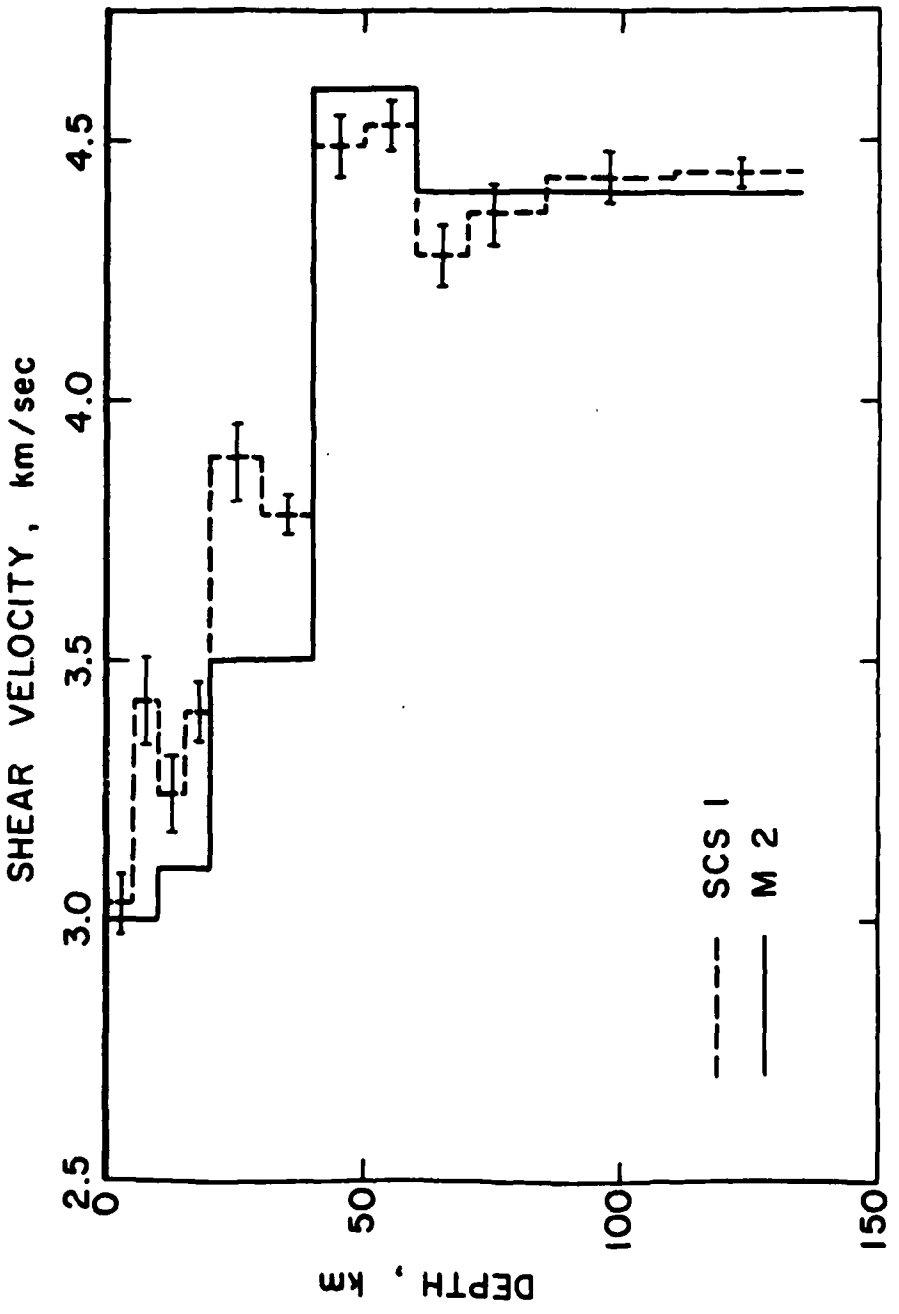
SHEAR VELOCITY, km/sec
2.5
3.0
3.5
4.0
4.5
DEPTH, km
0
50
100
150
SCS I
M 2

FIGURE 13

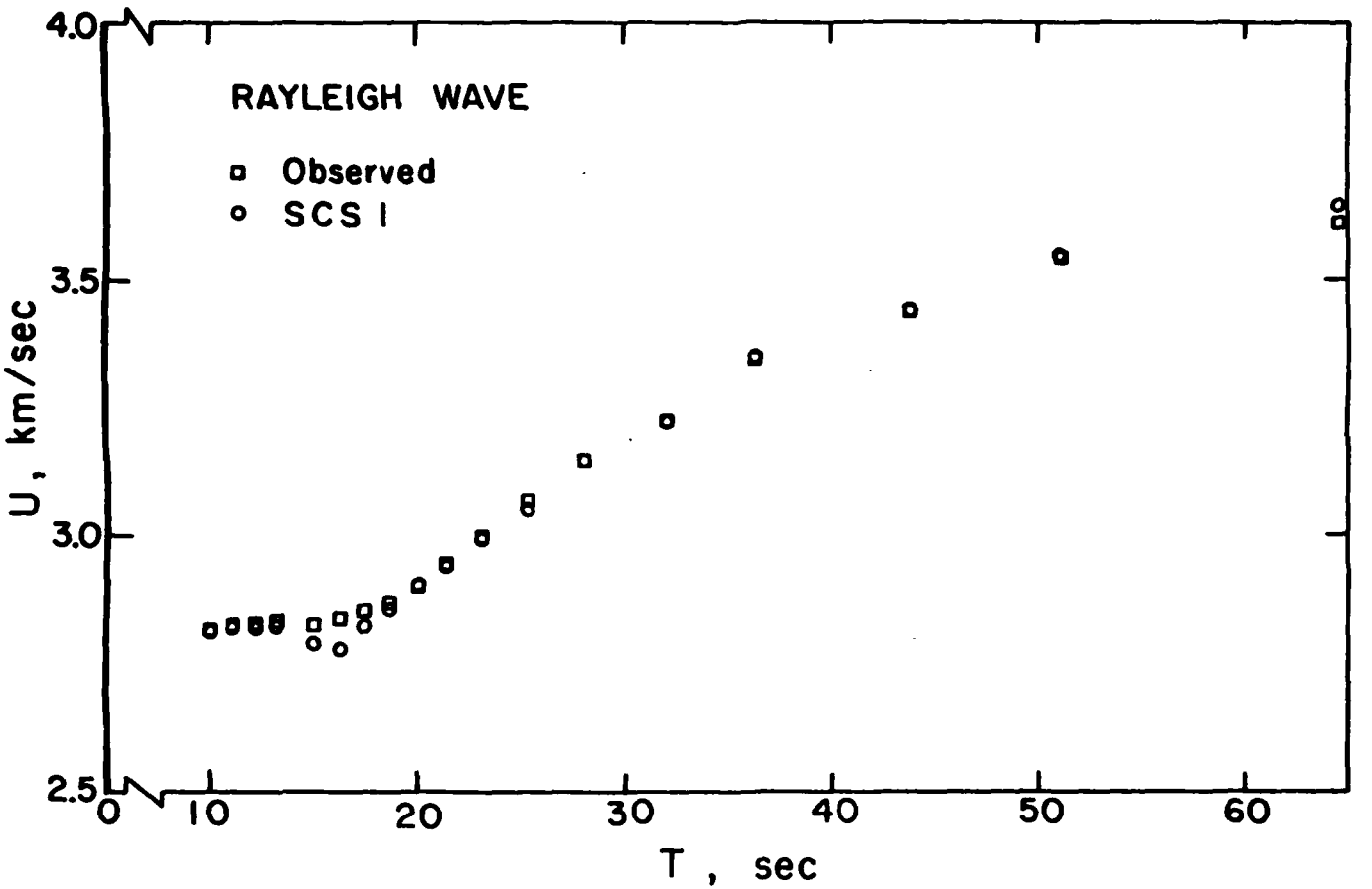
RAYLEIGH WAVE
Observed
SCS I
U, km/sec
4.0
3.5
3.0
2.5
0
10
20
30
40
50
60
T , sec

FIGURE 14

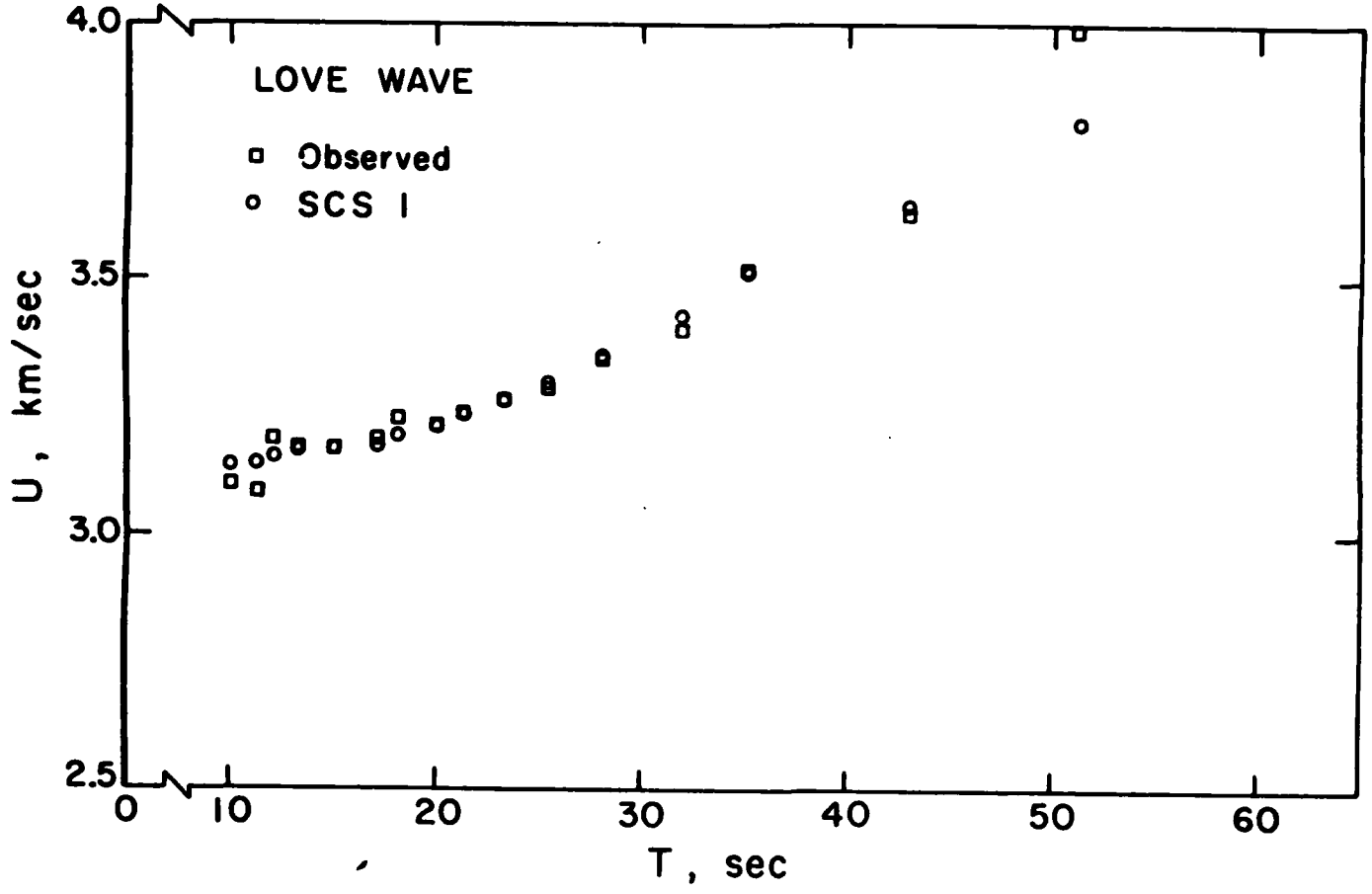
LOVE WAVE
Observed
SCS I
U, km/sec
T, sec
4.0
3.5
3.0
2.5
0
10
20
30
40
50
60

FIGURE 15

TABLE 7

RESOLVING MATRIX OF SHEAR PARAMETER

1.	.937	.096	-.058	.051	-.015	.008	-.002	.002	-.002	.001	.002	.002
2.	.096	.762	.259	.150	-.004	.030	-.004	-.014	-.006	-.002	-.003	-.003
3.	-.058	.260	.554	.316	-.016	-.065	.012	.026	.013	-.004	-.011	-.007
4.	.051	-.150	.317	.543	.184	-.056	-.051	-.009	.009	.008	-.002	-.004
5.	-.030	-.007	-.033	.368	.627	.281	-.017	-.087	-.054	-.019	-.001	-.009
6.	.015	.059	-.231	-.111	-.281	.526	.248	.080	-.081	-.074	-.055	-.024
7.	-.005	-.007	.040	-.101	-.017	.248	.315	.222	.103	-.003	-.055	.043
8.	.0042	-.028	.051	-.019	-.087	.080	.222	.281	.229	.092	-.030	-.057
9.	-.005	-.011	.027	.018	-.054	-.031	.103	.229	-.244	.168	.023	-.047
10.	.010	-.013	-.057	-.006	.003	-.137	-.137	-.076	.058	.170	.160	.055

a desired box car vector. An example would be if we wished to average the first two parameters, then we would want the kernal to resemble a box car function such as described in Table 8a. In the inversion, shear wave parameters from layers 2, 3 and 4 were averaged, as were parameters from layers 5 and 6, and layers 7 and 8, Table 8c. The actual kernals for these averaged parameters are shown in Table 8b. The averaged values and standard deviations are plotted in Figure 16. (Model ASCS1, Table 9). A comparison with Tung and Teng (1974) results indicates here that crustal shear velocities are higher than previously reported values. And the lid velocity in the mantle is found to be slightly less than previously determined. A LVL at 60 km is consistent with our dispersion data.

A list of the apriori and postpriori standard deviations for SCS1 is given in Table 10. There is almost no new information that can be derived from the data past 70 km. In the mantle in general, the amount of new information from the data is quite small. But the persistence of the LVL at the 60-70 km depth might indicate a true velocity reversal and possibly the transition between the lithosphere and asthenosphere.

TABLE 8

BOXCAR KERNAL FOR PARAMETERS 8a
1 and 2

1	1	0	0	0	0	0	0	0	0	0	0

ACTUAL BOXCAR AVERAGING KERNALS 8b

.089	.973	1.13	.710	.164	-.09	-.034	.002	.017	.002	-.015	-.015
-.015	.052	-.163	.256	.91	.81	.231	-.007	-.085	-.087	-.56	-.033
-.001	-.035	.091	-.12	-.10	3.27	.54	.502	.332	.097	.055	.099

THEORETICAL BOXCAR AVERAGING KERNALS 8c

0	1	1	1	0	0	0	0	0	0	0	0
0	0	0	0	1	1	0	0	0	0	0	0
0	0	0	0	0	0	1	1	0	0	0	0

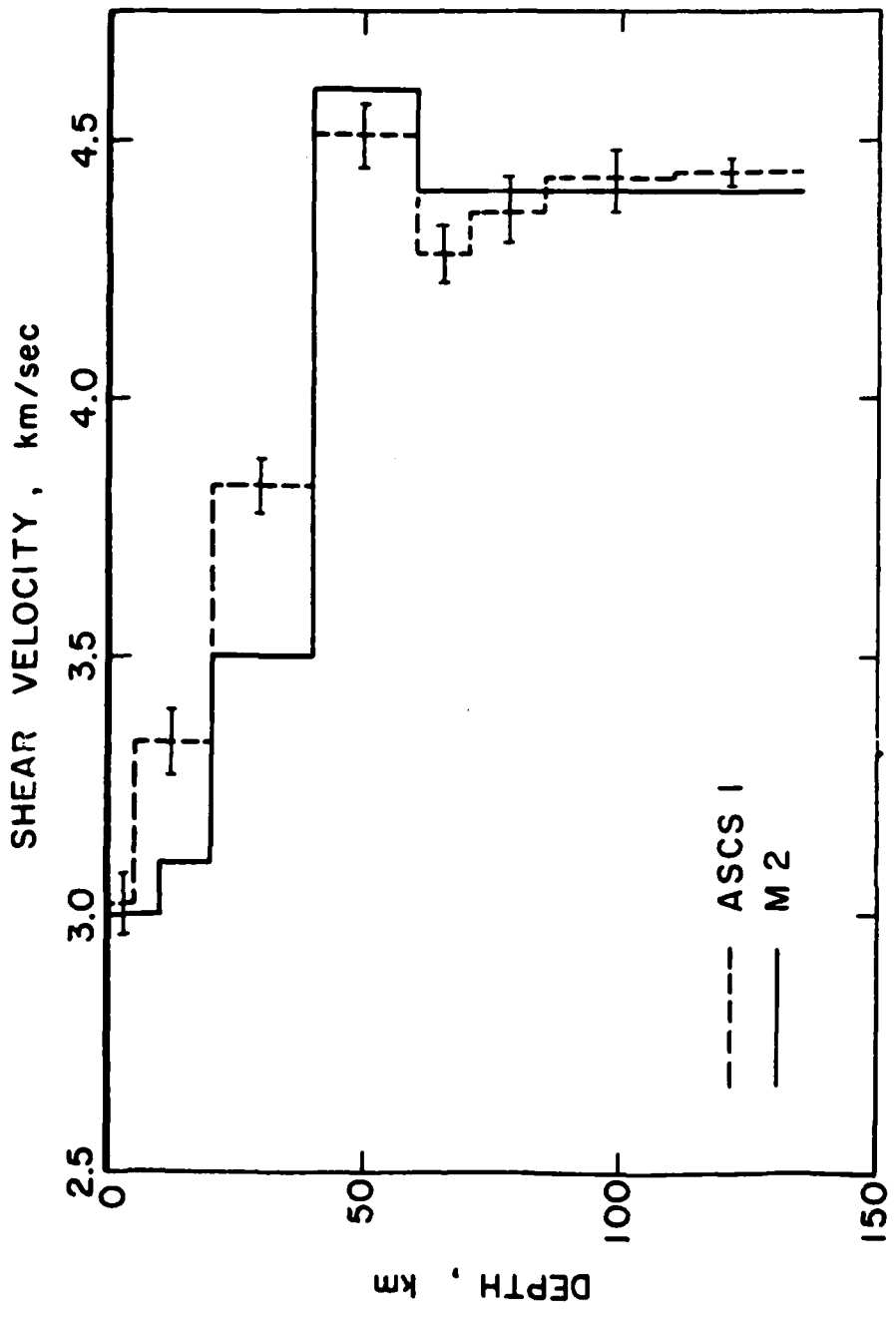
SHEAR VELOCITY, km/sec
2.5
3.0
3.5
4.0
4.5
0
50
100
150
DEPTH, km
ASCS I
M 2

FIGURE 16

TABLE 9

MODEL ASCS 1

LAYER THICKNESS (KM)	SHEAR VELOCITY (KM/SEC)	SDX_0	SDX
5	3.03	.347	.087
15	3.36	.200	.062
20	3.84	.173	.063
20	4.51	.173	.120
10	4.28	.245	.210
15	4.36	.200	.175
25	4.44	.155	.142
25	4.44	.155	.150

TABLE 10

FINAL MODEL
SCP1

SHEAR VELOCITY	SDX_0	SDX
3.03	.347	.087
3.43	.347	.169
3.24	.347	.231
3.4	.347	.234
3.89	.245	.150
3.78	.245	.169
4.49	.245	.203
4.53	.245	.210
4.28	.200	.175
4.36	.155	.142
4.35	.155	.150

CONCLUSIONS

By comparing the size of the P-wave partial derivatives with density and shear wave partial derivatives, it was determined that compressional wave velocity cannot be neglected when inverting surface wave data. The resolution for shear velocity is better than the resolution for density and p-wave velocity.

The inversion of multi-layer models indicates that a 3 layer, 40 km crust adequately describes the South-China subplate. The resolution ranged from 5 to 20 km in the crust with model standard deviations of less than .08 km/sec. The shear velocities were found to be higher than those velocities reported by Tung (1974).

Upper mantle shear velocities were found to be lower than previously reported values. Resolution in the mantle was quite poor as no dispersion information is obtained from this study beyond 65 seconds. The apriori and postpriori standard deviation indicated that very little new information was being obtained from the data about the mantle. But because of the persistence of a LVL between 60 and 70 km, it is presumed that transition between the lithosphere and asthenosphere occurs here.

REFERENCES

REFERENCES

Backus, G. and Gilbert, F. (1967). Numerical Application of a Formalism for Geophysical Inverse Problems: Geophys. J. 13, p. 247-276.

Backus, G. and Gilbert, F. (1968). The Resolving Power of Gross Earth Data: Geophys. J. 16, p. 169-205.

Braile, L. W. and Keller G. R. (1975). Fine Structure of the Crust Inferred from Linear Inversion of Rayleigh Wave Dispersion: Bull. Seism. Soc. Am., 65, p. 71-82.

Crossen, R. S. (1976). Crustal Structure Modeling of Earthquake Data 1, Simultaneous Least Squares Estimation of Hypocenter: J. Geophys. Res., 81, p. 3030-3046.

Der, Z. Masse, R. and Landisman, M. (1970). Effects of Observational Errors on the Resolution of Surface Waves at Intermediate Distances: J. Geophys. Res. 75, p. 3399-3409.

Der, Z., and Landisman, M. (1972). Theory for Errors, Resolution, and Separation of Unknown Variables in Inverse Problems, with Application to the Mantle and Crust in Southern Africa and Scandinavia: Geophys. J., 27, p. 137-179.

Dziewonski, A. and Hales, A. L. (1972). Numerical Analysis of Dispersed Seismic Waves: Method in Computational Physics, v. II, Academic Press, p. 306.

Dziewonski, A., Bloch, S., and Landisman, M. (1969). Technique for the Analysis of Transient Seismic Signals: Bull. Seism. Soc. Am., 59, p. 427-444.

Franklin, J. N. (1970). Well-Posed Stochastic Extensions of Ill-Posed Linear Problems: J. Math. Anal., 31, p. 682-716.

Hanson, R. J., and Lawson, C. L. (1973). Solving Least Squares Problems, Prentice Hall, Englewood Cliffs, N. J., p. 18-23.

Hermann, R. B. (1973). Some Aspects of Band-Pass Filtering of Surface Waves: Bull. Seism. Soc. Am., 63, p. 663-671.

Jackson, D. D. (1972). Interpretation of Inaccurate, Insufficient, and Inconsistent Data: Geophys. J. Roy. Astron. Soc., 28, p. 97-109.

Jordan, T. H., and Franklin, J. N. (1971). Optimal Solutions to a Linear Inverse Problem in Geophysics: Proc. Nat. Acad. Sci. U.S., 68, p. 291-293.

Kuichow Geologic Team 108 (1975). Features of Bedded Ultrabasic Rocks in Fairhinshun Region of Kuichow Province and a Preliminary Disucssion of their Origin: Scientia Geologica Sinica, 4, p. 343-351.

Li, C. Y. Cai, W. B., Ding, M. L., Xu, I. M., and Wang, Y. P. (1974). A Note on the Seismo-Geologic Features in China: Scientia Geologica Sinica, 1, p. 357-370.

Lee, W. H., Wu, F. T. and Jacobsen, C. (1976). A Catalog of Historical Earthquakes in China Compiled from Recent Chinese Publications: Bull. Seism. Soc. Am., 66, p. 2003-2016.

Sun, N. C. and Teng, T. (1977). Tectonic Plates of China: University of Southern California, Geophysical Laboratory Technical Report, 77-4.

Sung, C. H., Ho, G. T. and Hsu, G. M. (1965). A Study of the Sedimentary Layers in China: Acta Geophysica Sinica, 14, p. 158-167.

Tseng, J. S. and Sung, Z. A. (1963). Phase Velocity of Rayleigh Waves in China: Acta Geophysica Sinica, 12, no. 2, p. 148-165.

Tung, J. P. (1974). The Surface Wave Study of Crustal and Upper Mantle Structure of Mainland China: Ph.D. dissertation, University of Southern California, 248 p.

Wiggins, R. A., (1972). The General Linear Inverse Problems: Implications of Surface Waves and Free Oscillations for Earth Structure: Rev. Geophys. Space Phys., 10, p. 251-285.

APPENDICES

APPENDIX I

In tis appendix attention will be focused primarily on how to use the computer programs discussed in this thesis. There are very little mathematical and algorithmic descriptions given in this text. These descriptions are covered in the reference section in Table A.1, and it is to the benefit of the user to read these papers before attempting to use the programs. The algorithms have been tested and implemented in Fortran 4, with the entire set of codes presented in card image format or set into a load module.

The 3 main programs, PLOT, GVA (group velocity analysis) and SWI (surface wave inversion), are presented here in the order used in the actual surface wave inversion process.

PLOT

After obtaining the SRO data tapes, the problem is to put the data into a recognizable form; this is accomplished by the program PLOT.

A. Deck Setup.

Figure A.1 shows the order of cards in the deck. The only cards that need to be changed are the input cards and the "VOL=SER=" card. The "VOL=SER=XXX" number is simply the storage location or "bin" number at the University Computer Center. It tells

TABLE A.1

PROGRAM	DESCRIPTION	REFERENCE
PLOT	Rotates and plots seismogram	---
GVA	Group velocity analysis of rotated seismogram	Tung (1974) and Hermann (1972)
SWI	Does actual surface wave inversion to obtain theoretical earth model	Wiggins (1972) and Jackson (1972)

```
INPUT DATA DECK
//GO, SYSIN DD *
//GO, SYSPUNCH DD SYSOUT=B, DCB=BLKSIZE=80
//DCB=(RECFM=FB, LRECL=2000, BLKSIZE=2000)
//GO, FT08F001 DD VOL=SER=XYZ1, UNIT=6200BPI,DEFER), LABEEL=(1,NL),
//GO, FT21001 DD SYSOUT=X DCD=LRECL=504, BLKSIZE=3156, RECFM=VBS
FORTAN PROGRAM DECK
//FORT.SYSIN DD *
//EXEC FORTGCLG, RG=120K, TIME=5
//*UCC CORE=120K, TIME=5, CHARGES=ALL
CARD 1 → JOB CARD
```

FIGURE A.1

the operator where to find your tape.

B. Input Cards.

Input cards and their formats are listed below.

Card 1 FORMAT (F5.2)

THETA = the angle coordinate axes rotation

Card 2 FORMAT (2(I4,6X))

IFIRST = the value of the first SRO data record to be read in

NDATA = number of data points to be plotted (maximum = 2000, if ISKIP = 0)

Card 3 FORMAT (2(I4,6X)

ISKIP = the number of short-period records that are skipped to get to the next long-period record

NEXTRA = the number of extra data points to be plotted. There can be more than, but NEXTRA + NDATA cannot be greater than 2000.

Card 4 FORMAT (2(I4,6X))

ISTRT = the point at which the user wants punched output to begin

PNCH = the number of points to be punched

C. Output.

The output consists of three plots (for an example see Figure 3). If punched data is requested then output will have the format (5(I4,E12.6)). The vertical, north-south, and east-west component punched output are separated by a blank card and a card that says "NUM = ." The punched output is ready to use in the multiple-filtering program, GVA.

GVA

The multiple-filtering analysis of the digitized surface wave train, is accomplished in the program GVA.

A. Deck Setup.

Figure A.2 shows the order of cards in the deck. The only cards that need to be changed are the input cards.

B. Input Cards.

Input cards and their format are listed below.

Card 1 FORMAT (20A4)

NAME = an alphanumeric description of the data

Card 2 FORMAT (I5, f5.0)

LX = the total number of data points to read in (this value has to equal 2**N

```
INPUT DATA DECK
//GO, SYSIN DD*
//GO, SYSPUNCH DD SYSOUT=B, DCB=BLKSIZE=80
FORTRAN PROGRAM DECK
//FORT, SYSIN DD *
//EXEC FORTGCLG, RG=240K, TG=2
//* UCC CORE=240K, CHARGES=ALL, LINES=10, TIME=2
CARD 1 → JOB CARD
```

FIGURE A.2

DX = The digitization interval (for SRO long-period data this value equals 1)

Card 3 FORMAT (2F10.3)

DIST = the epicentral distance

TCON = the difference between the earthquake origin time and the time at the start of the first record using in program PLOT

Card 4

X(I) = punch output of PLOT

Y(I) = punch output of PLOT

C. Output

The most important part of the output is a plot of the group velocity vs. period. (For an example see Figure 5.)

D. Problems using GVA

1. Make sure there are 2**n data points (where n is some integer value)
2. Have punched output from that part of the seismogram which represents the group velocity arrivals between 4.5 km/sec and 2.0 km/sec.
3. You might have higher mode arrivals in your dispersion curve. This is not a problem. Try to identify these arrivals and use them

```
INPUT DATA
//STEPLIB DD DSN=RGH01.LOAD, SISP=SHR
//FT61001 DD DUMMY
//FT61F001 DD UNIT=SYSTEMP, SPACE=(CYL,1), DSN=88BB
//DCB=CRECFM=VBS, LRECL=500, BLKSIZE=1504)
//FT51F001 DD UNIT=SYSTEMP, SPACE=(CYL,(5,2)), DSN=S8AA
//FT07F001 DD DUMMY
//FT06F001 DD SYSOUT=A
//FT05F001 DD DDNAME=SYSIN
//MYJOB EXEC PGM=BOB, REGION=320K, TIME=25
//* UCC CORE=320K, TIME=25, CHARGES=ALL, LINES=30
CARD 1 → JOB CARD
```

FIGURE A.3

in your inversion.

4. If you have plotted the seismogram, (p wave, s wave, and surface wave arrivals) TCON might be negative. Input this the same way you would for any F type format.

SWI

SWI takes the group velocity data obtained in GVA and inverts it for an earth model. The program has been set up into a load module. Therefore, the only part of the program that has to be submitted to the computer is the input data deck and some job control language cards, Figure A.3.

The comment cards in the listing of SWI give an excellent description of the different input and output parameters (Appendix 3). This listing also shows how to input the data into the load module. The discussion here will be limited to the problems in using the program.

A. Problems in using SWI

1. Invert for shear velocity, and density. If you have a problem in obtaining a reasonable final model, then invert for compressional velocity also.

2. When choosing values for "TOP" use values like 10^{-1}, 10^{-2}, 10^{-3}, and 10^{-4}. Do not

use values in between these. Probably the smallest value you will need to try is 10^{-4}. I found that 3 or 4 iterations at 10^{-3} got the necessary RMSFIT.

3. You want your final RMSFIT at less than 1. But anything up to a RMSFIT of 1.5 is probably reasonable.
4. Remember we are trying to get stable models. Stability is achieved when all your PNMPG are less than STDEV K.

APPENDIX II

In this section an illustration is given on how to use the programs.

EXAMPLES

An earthquake occurred in the Szechwan Province of mainland China and was recorded at station TATO. The origin time was 9/1/76, 1:6:51.8, and the epicentral distance is 1886.28 km.

PLOT

The angle of axis rotation was found to be 21.7^0. We now want to know when the surface wave arrives at TATO. Divide the epicentral distance by 4.5 km/sec and add this value to the origin time. This value equals 1:13:27.6. Now find out when this time occurs in the SRC datatape. In our example, the first arrival occurs in record 240.

GVA

We now have punched output from PLOT and wish to get a dispersion curve. We know that the epicentral distance is 1886.28. To get TCON subtract the origin time by the starting time of record 240; this value equals 336.1. It should be noted that I only have punched output from 150-450 seconds, a total of 301 points. But I need 512 points (2**9). This problem is remedied by adding on the

end of the punched output (from 451-661) a set of points whose amplitude values equal zero.

APPENDIX III

In this section the input data sequence is given for the surface wave inversion program (Rodi, 1977).

A. Input Cards

Card 1 FORMAT (8I2,2E8.0.3F8.0)

LEAST = Flag controlling how calculations are done. Normally use LEAST = 0 for NPARM>NDATA, LEAST = 1 otherwise

NITERX(1) Number of iterations using ALF TOP on this card

NALF Number of extra ALF/TOP pairs read in later

IFVX FLAG IFVX = 1 Calculate and print out 'St Dev x'

= 0 Don't do it

IFVK FLAG IFVK = 1 Calculate and print out 'St Dev k'

= 0 Don't do it

IFKERN FLAG IFKERN= 2 Print and punch averaging kernals

= 1 Print averaging kernals

= 0 Don't do it.

NJUMP = Number of numbers on card 12, which describes which parameters

not to calculate variances for

NORM FLAG NORM = 1 Normalize averaging kernals read in later

= 0 Take averaging kernals read in later as is

TOPX(1) Value of TOP. If TOP>0 it is used to compute ALF

ALFX(1) Value of ALF

QUIT1 Stopper. It stops iterating when RMSFIT<QUIT1

QUIT2 Stopper. It stops iterating when RMSFIT(present)>Quit 2*RMSFIT (last)

THRESH Print/punch only the averaging kernals for which 'QK'<THRESH

If NALF>0, then read in .NALF. cards of Card 2

Card 2 FORMAT (2X,I2,12X,2E8.0)

NITERX Number of iterations using ALF/TOP on this card. If NITERX = 0, then (1) subsequent Card 2's must have NITREX = 0, and (2) parameter corrections gotten using this. ALF/TOP will not be used to get

final model. NITERX=0 is used to get RX-STDEVX and QK-STDEVK trade-off curves for next-to-last model.

TOPX Value of TOP

ALFX Value of ALF

Card 3 FORMAT (5I1,I3)

IFLATR	FLAG	IFLATR=1	Do sphericity correction for Rayleigh using 'Biswas Earth flattening'
		=0	Don't do it
IFLATL	FLAG	IFLATL=1	Do sphericity correction for Love using "Biswas Earth flattening'
		=0	Don't
IFDIS	FLAG	IFDIS =1	Print out the layer displace-ments
		=0	Don't do it
IFENG	FLAG	IFENG =1	Print out the layer energy
		=0	Don't do it
IFPAR	FLAG	IFPAR =1	Print out the

layer partial
derivatives W.R.T.
layer parameters

=0 Don't do it

KEEP Plus or minus a data set reference no. (say a tape unit) for saving inversion results. For example:

KEEP=91: Save inversion results as of last iteration

KEEP=-91: Save this and data and partials for final model

KEEP=0: Save nothing

Note: Data and partials for final model are only computed if they are requested to be saved

Card 4 FORMAT (18A4)

ID Alphanumeric data descriptor

Card 5 FORMAT (I4,2I1,2F8.0)

NDATA Number of data.

LOGD FLAG LOGD=1 Inverse program uses natural log of C & U for observations, so read in standard devs of log C or log U

=0 C and U are used for observations

IFTORF FLAG IFTORF=2 Velocities are functions of period

=3 Velocities are functions of frequency

DTFLOG Pertubation of log frequency used to compute U-partials. .001 is a good value

STEP Trail phase velocity increment/ decrement

Number of card 6's = number of frequencies

Number of card 7's = number of data

Card 6 FORMAT (4I1,2F8.0)

KINDX FLAG KINDX=1 For Rayleigh Wave

=2 For Love Wave

MODEX Mode number, i.e., 0 for the fundamental mode, 1 for the first higher mode and so on.

IFCUX(1) FLAG IFCUX(1)=1 Read in phase velocity.

=0 No.

IFCUX(2) FLAG IFCUX(2)=1 Read in group velocity.

=0 No.

IF — Period for IFTORF=2 or frequency for IFTORF=3.

Start — Guess root (Phase velocity) for the period/frequency.

There follow .IFCUX(1) + IFCUX(2). Cards of Card 7

Card 7 FORMAT (F8.0,I4,5(I4,F8.0)/(6(I4.F8.0))

DOBS — Observed value of phase(C) or group(U) velocity

NVAR — Number of data this obs has covariances with (including itself but not data already read in)

MAP — Datum number this obs covaries with minus datum number of this obs (thus Map=0 means variance)

ED — Value of standard deviation (co-deviation). If MAP>0: Codev = Sign(covar)*SQURT(Abs(Covar)).

Card 8 FORMAT (18A4)

ID — Alpnanumeric model descriptor.

Card 9 FORMAT(I4,4I1)

Layers — Number of layers including water layer and half space in the guess model.

LOGP FLAG LOGP =1 Inverse prog uses

log VP, VS, density as parameters.

=0 VP, VS, Density used as parameters.

IFVP FLAG IFVP =1 Invert for P-wave velocity (VP)

=0 No.

IFVS FLAG IFVS =1 Invert for S-wave velocity (VS)

=0 No.

IFDEN FLAG IFDEN =1 Invert for density

=0 No.

There now follow .layers. cards of card 10

Card 10 FORMAT (4F10.4)

HQ Layer thickness in km.

ALPQ Layer P-Wave velocity in km/sec.

BETQ Layer S-Wave velocity in km/sec.

RHOQ Layer density in gm/cc.

There now follow .IFVP + IFVS + IFDEN. Sets of card 11. Number of cards in each set depends on how the user divides the model into segments.

Card 11 FORMAT (I4,2F8.0)

LAY2 Number of bottom layer of segment using WIDTH and DEV given on this card.

WIDTH Smoothing interval in km.
Recommendation: Set WIDTH = 0.

DEV If WIDTH = 0, DEV**2/ALF is assumed variance per km of parameters in this segment.
Note: Absolute size of DEV is unimportant. Relative sizes of DEV in different segments allows constraining of some parameters compared to others. (Small DEV=>Big constrain.) Absolute degree of constraining can be controlled with ALF. (Big ALF = >Big Constrain.)

If NJUMP not equal to zero, use card 12

Card 12 Free FORMAT (Use only columns 1-72)
On this card are NJUMP Numbers which indicate the parameters for which variances and averaging kernels are not to be calculated. For example, if NJUMP = 4 and this card contains 1, -22, 25, and +30, then they won't be done for parameters 1 through 22, parameter 25 and parameter 30. The '+' sign before 30 can be omitted.

Card 13 Free FORMAT (Use only columns 1-72)
This card contains an ideal averaging kernal

(the vector X). Example: 4*0 10*.1 999*0. This vector averages parameters 5 through 14.